

1 **Cellular profiling of a recently-evolved social behavior**

2 Zachary V. Johnson^{1,2,*}, Brianna E. Hegarty^{1,2,*}, George W. Gruenhagen^{1,2,*}, Tucker J. Lancaster^{1,2}, Patrick T.
3 McGrath^{1,2,†}, Jeffrey T. Streebman^{1,2,†}

4
5 ¹School of Biological Sciences, Georgia Institute of Technology, Atlanta, GA 30332

6 ²Institute of Bioengineering and Bioscience, Georgia Institute of Technology, Atlanta, GA 30332

7 * these authors contributed equally to this work

8 † corresponding authors

9
10 Correspondence: todd.streebman@biology.gatech.edu, patrick.mcgrath@biology.gatech.edu

11 **ABSTRACT**

12
13
14 Social behaviors are essential for survival and reproduction and vary within and among species. We integrate
15 single nucleus RNA-sequencing (snRNA-seq), comparative genomics, and automated behavior analysis to
16 investigate a recently-evolved social “bower building” behavior in Lake Malawi cichlid fishes. We functionally
17 profile telencephalic nuclei matched to 38 paired behaving/control individuals. Our data suggest bower behavior
18 has evolved in part through divergence in a gene module selectively expressed in a subpopulation of glia lining
19 the pallium. Downregulation of the module is associated with glial departure from quiescence and rebalancing
20 of neuronal subpopulation proportions in the putative homologue of the hippocampus. We show further
21 evidence that behavior-associated excitation of neuronal populations that project to the putative hippocampus
22 mediate glial function and rebalancing. Our work suggests that bower behavior has evolved through changes
23 in glia and region-specific neurogenesis, and more broadly shows how snRNA-seq can generate insight into
24 uncharted behaviors and species.

25 INTRODUCTION

26 Social behaviors vary tremendously within and among species, and they are disrupted in heritable human brain
27 diseases (Johnson and Young 2017; Kennedy and Adolphs 2012). Many social behaviors are not expressed
28 in standard laboratory models, and much progress in understanding the biological mechanisms of social
29 behaviors has been made through work in diverse and non-traditional species systems (S. Juntti 2019; Gallant
30 and O’Connell 2020; Laurent 2020; Keifer and Summers 2016; Brenowitz and Zakon 2015; Jourjine and
31 Hoekstra 2021; Johnson and Young 2018). Different experimental traditions spanning genomics (C. R. Smith
32 et al. 2008; Küpper et al. 2016; Lamichhaney et al. 2016; Bendesky et al. 2017; York et al. 2018; Pfenning et
33 al. 2014; Dias and Walsh 2020; Stein et al. 2017), endocrinology (S. A. Juntti et al. 2016; Boender and Young
34 2020; Adkins-Regan 2013; O’Connell, Matthews, and Hofmann 2012; S. Ogawa et al. 2000; Heinrichs and
35 Gaab 2007; Schiller, Meltzer-Brody, and Rubinow 2015), and circuit neuroscience (Gutzeit et al. 2020; Hung
36 et al. 2017; Amadei et al. 2017; Anderson 2016; Gangopadhyay et al. 2021; Kohl et al. 2018; S. B. Nelson and
37 Valakh 2015; Bachevalier and Loveland 2006) have contributed to our understanding of social behavior.
38 However, we still have a poor understanding of the genetic and cellular pathways through which social
39 behaviors vary and evolve. Discovering these gene-brain-behavior links is necessary to understand how neural
40 circuit functions vary during social contexts.

41 Single cell omics technologies enable simultaneous profiling of many heterogeneous cell populations in any
42 species with a reference genome, eroding important historical barriers that have faced investigation of new
43 social behaviors and species systems. These technologies have already advanced our understanding of the
44 brain (Tosches et al. 2018; Jerber et al. 2021; Raj et al. 2018; M. Zhang et al. 2021), however, to our knowledge
45 only one study has used single cell omics to functionally profile the brain during behavior (Moffitt et al. 2018).
46 Here we integrate single nucleus RNA-sequencing (snRNA-seq) with automated behavior analysis and
47 comparative genomics to investigate the neurobiological substrates of a recently-evolved (<1 Mya) social bower
48 construction behavior in Lake Malawi cichlid (*Cichlidae*) fishes. Cichlids are teleost (*Teleostei*) fishes, a group
49 representing ~40% of all living vertebrate species (Salzburger 2018). As teleosts, cichlids possess predicted
50 homologues for ~80% of human disease-associated genes (Howe et al. 2013). In the brain, teleosts and
51 mammals share conserved neuronal and non-neuronal cell populations with conserved molecular,
52 electrophysiological, morphological, transcriptional, and behavioral properties (O’Connell and Hofmann 2011b;
53 Xie and Dorsky 2017; Elliott et al. 2017; Jurisch-Yaksi, Yaksi, and Kizil 2020). For example, the teleost
54 telencephalon contains conserved cell populations that are thought to regulate social behaviors across diverse
55 vertebrate lineages (O’Connell and Hofmann 2011b).

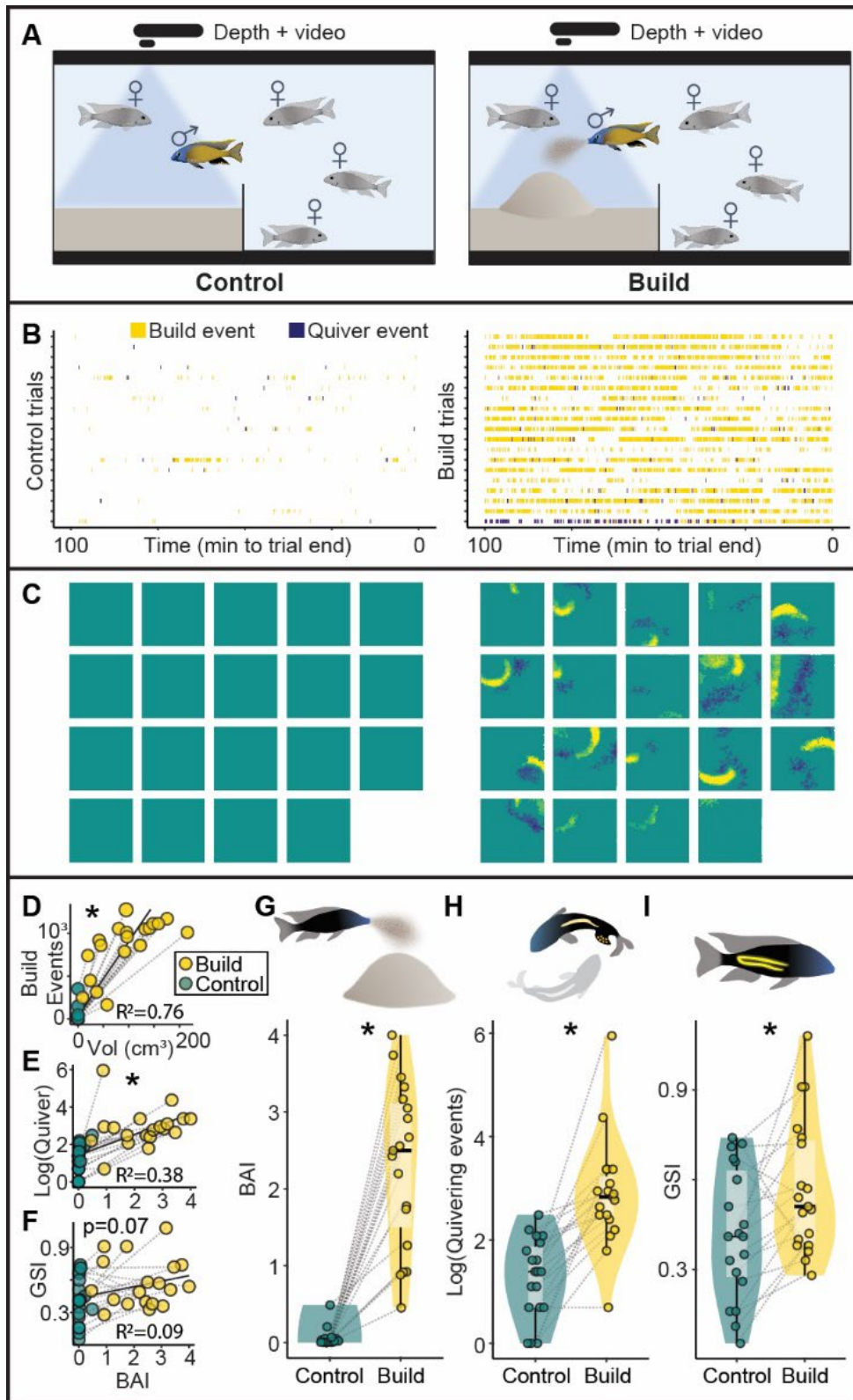
56 Lake Malawi is home to ~800 cichlid species are behaviorally diverse (York et al. 2015; Baran and Streelman
57 2020; Ribbink et al. 1983; Johnson, Moore, et al. 2020; York et al. 2018) but genetically similar (Loh et al. 2008;
58 Malinsky et al. 2018), thus representing a powerful system for investigating the neurogenetic basis of behavioral
59 variation. In ~200 species, males express bower construction behaviors during the breeding season, during
60 which they repetitively spatially manipulate sand into species-specific structures for courtship and mating (York
61 et al. 2015; Johnson, Arrojjwala, et al. 2020; Long et al. 2020). Many species dig crater-like “pit” depressions
62 while others build volcano-like “castle” elevations, and these behavioral differences are associated with
63 genomic divergence in a ~19 Mbp chromosomal region enriched for human disease-associated genes and
64 genes that exhibit *cis*-regulated behavior-associated expression in the cichlid brain (York et al. 2018).

65 In this paper we investigate castle-building behavior in *Mchenga conophoros*, a Lake Malawi cichlid and an
66 uncharted species in behavioral neuroscience. We use natural genetic differences among individuals to link
67 single nuclei back to 38 paired behaving/control test subjects, enabling measurement of building-associated
68 signals and simultaneous control for two additional biological variables that may influence brain gene
69 expression: quivering, a courtship “dance” behavior, and relative gonadal mass. We first map the cellular
70 diversity of the telencephalon and then investigate cell type-specific signatures of active castle-building
71 behavior as well as genomic divergence associated with behavioral evolution. Our work shows how snRNA-
72 seq profiling can generate converging lines of evidence for candidate genes, molecular signaling systems, cell
73 populations, and brain regions underlying social behaviors in uncharted species systems.

74 RESULTS

75 Castle-building is associated with increased quivering behavior and gonadal physiology

76 We used an automated behavior analysis system (Johnson, Arrojjwala, et al. 2020; Long et al. 2020) to monitor
77 reproductive adult *Mchenga conophoros* males as they freely interacted with four reproductive adult females
78 and sand (Fig. 1A). This system uses depth sensing to measure structural changes across the sand surface
79 and action recognition to predict building and quivering (a stereotyped courtship “dance” behavior) from video
80 data. We sampled pairs of males at the same time in which one male was actively castle-building within the
81 past two hours (n=19) and the other was not (“control”, n=19; Fig. 1B-C). For each subject, we also recorded
82 the gonadal somatic index (GSI), a measure of relative gonadal mass that is correlated with gonadal steroid
83 hormone levels and social behaviors in cichlids (Maruska and Fernald 2010; Ramallo et al. 2015; Alward et al.
84 2019) (Table S1). The volume of sand displaced by males was positively correlated with the number of building
85 events predicted from video data by action recognition (Fig. 1D). For simplicity, we combined depth and action
86 recognition data into a single “Bower Activity Index” (BAI). Building males had greater BAIs, quivered more,
87 and had greater GSIs (Fig. 1E-I) compared to controls. Taken together, these results are consistent with castle-
88 building, like many social behaviors in nature, being embedded within a suite of behavioral and physiological
89 changes tied to reproduction.



90

91 **Figure 1. Castle-building is associated with increased quivering and relative gonadal mass.** (A)
 92 Schematic of behavioral assay, 19 pairs of building (right) and control (left) males were sampled. Action
 93 recognition (B, yellow=building, blue=quivering, each trial is represented by a row, with pairs matched by row
 94 between left and right panels) and depth sensing (C, yellow=elevations, blue=depressions, each square
 95 represents total depth change for one trial, with pairs matched by row and column between left and right panels)
 96 revealed behavioral differences between building and control males. (D) Structural change measured through
 97 depth sensing (adjusted for body size) was strongly and positively correlated with building behaviors predicted
 98 through action recognition ($p=8.15 \times 10^{-13}$), and these measures were combined into a single Bower Activity

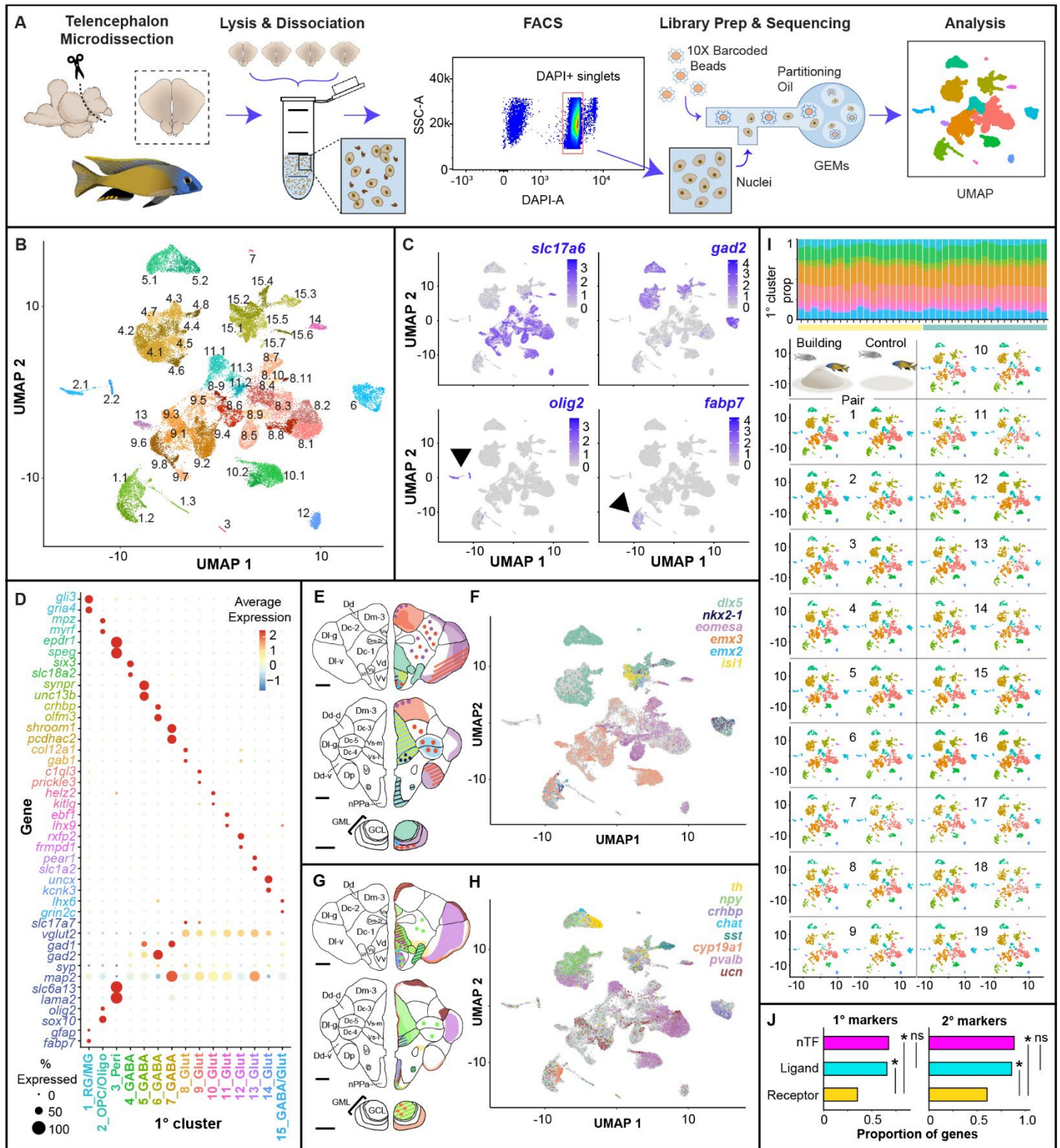
99 Index (BAI, x-axis in E and F). BAI was positively correlated with quivering behaviors (E, $p=3.35 \times 10^{-5}$), and
100 trended toward a positive correlation with GSI (F, $p=0.07$). Compared to controls, building males exhibited
101 greater BAIs (G, 4.24×10^{-8}), quivering (H, $p=9.18 \times 10^{-6}$), and GSIs (I, $p=0.0142$). Gray lines in panels D-I link
102 paired building and control males.

103 **Telencephalic nuclei reflect major neuronal and non-neuronal cell classes**

104 Telencephala (n=38) were combined into ten pools (n=5 behave, n=5 control, 3-4 telencephala/pool) for
105 snRNA-seq (Fig. 2A). >3 billion RNA reads were sequenced and mapped to the Lake Malawi cichlid *Maylandia*
106 *zebra* reference genome (Conte et al. 2019). 33,674 nuclei (~900 nuclei/subject) passed quality control filters
107 and were linked back to test subjects using genomic DNA. Coarse-grained clustering grouped nuclei into 15
108 “primary” (1°) clusters and finer-grained clustering grouped nuclei into 53 “secondary” (2°) clusters (ranging
109 from 57-1,905 nuclei, Fig. 2B). Established marker genes revealed known neuronal and non-neuronal cell types
110 (Fig. 2C), including excitatory (*slc17a6+*) and inhibitory (*gad2+*) neurons, oligodendrocytes and oligodendrocyte
111 precursor cells (OPCs, *olig2+*), radial glial cells (RG, *fabp7+*), microglia, pericytes, and hematopoietic stem
112 cells (Table S2). Unbiased analysis identified genes exhibiting nearly cluster-exclusive expression (Fig. 2D, top
113 rows). Different clusters also exhibited preferential expression of genes encoding transcription factors (TFs;
114 Fig. 2E-F) and neuromodulatory signaling molecules (Fig. 2G-H) that exhibit conserved neuroanatomical
115 expression patterns in teleosts (Table S2). (Fig. 2I, Table S3). Cluster composition was relatively consistent
116 across individuals. For clarity, we assigned each 1° cluster a numeric identifier (1-15) followed by a label
117 indicating one or more of these cell classes (e.g. for radial glia, “_RG”). 2° cluster labels were rooted in these
118 1° labels, but with a second numeric identifier indicating the relative size within the corresponding “parent” 1°
119 cluster (e.g. “4_GABA” is a 1° cluster expressing inhibitory neuronal markers, and “4.3_GABA” is the third
120 largest 2° cluster within 4_GABA). Marker genes for every individual 1° and 2° clusters were independently
121 enriched ($q < 0.05$) for eight GO categories related to cell morphology, connectivity, conductance, and signal
122 transduction (Table S4), supporting these as additional axes distinguishing clusters in this study. Cluster marker
123 genes were also more strongly enriched for genes encoding conserved brain region-specific
124 neurodevelopment/neuroanatomy-associated TFs (nTFs, n=43) and ligands (“ligands”, n=35) compared to
125 neuromodulatory receptors (“receptors”, n=108, Table S5; receptors versus nTFs, $p \leq 8.33 \times 10^{-4}$ for both 1° and
126 2° clusters, FET; receptors versus ligands, $p \leq 0.0068$ for both; nTFs versus ligands, $p \geq 0.75$ for both, Fig. 2J),
127 consistent with recent single cell RNA-seq (scRNA-seq) analyses of the mouse hypothalamus (Moffitt et al.
128 2018). Notably, several nTFs involved in dorsal-ventral patterning in early neural development exhibited striking
129 polarity in expression across clusters (Fig. 2F). For example, *dlx* genes and *isl1* mark the ventral telencephalon
130 while *emx* genes mark the dorsal telencephalon during the neurula stage (Sylvester et al. 2013), suggesting
131 that transcriptional signatures of developmental patterning are present in adult neurons. Together these data
132 may reflect organizing principles whereby transcriptional programs related to neurodevelopment and ligand
133 synthesis are less labile, while neuromodulatory receptors are expressed more promiscuously across cell
134 populations.

135

136



137

138

139

140

141

142

143

144

145

146

147

Figure 2. Molecular and cellular diversity of the cichlid telencephalon. (A) Schematic of experimental pipeline for snRNA-seq. (B) Nuclei cluster into 1° (n=15) and 2° (n=53) clusters. (C) Known marker genes reveal distinct clusters of excitatory neurons (*slc17a6*+), inhibitory neurons (*gad2*+), oligodendrocytes and oligodendrocyte precursor cells (*olig2*+), radial glia (*fabp7*+), as well as other less abundant cell types (not shown, see Table S2). (D) Clusters are distinguished by genes that exhibit near cluster-exclusive expression (top rows) as well as established cell type marker genes (bottom rows). Conserved nTFs (E, F) and ligands (and related genes; G, H) exhibit conserved neuroanatomical expression profiles in teleost fishes (E, G show schematic representations of conserved expression patterns), and show distinct expression in specific clusters. (I) Cluster proportions are consistent across 38 males (yellow and turquoise coded columns in top stacked bar chart represent building and control subjects, respectively). (J) nTF and ligand genes are differentially

148 overrepresented among 1° and 2° cluster markers compared to receptor genes. Anatomical figures adapted
149 with permission from Dr. Karen Maruska (Maruska et al. 2017).

150 **Building, quivering, and gonadal physiology are associated with signatures of neuronal excitation in**
151 **distinct cell populations**

152 To identify candidate cell populations that may regulate castle-building behavior, we first investigated
153 transcriptional signatures of neuronal excitation. Neuronal excitation triggers intracellular molecular cascades
154 that induce transcription of conserved immediate early genes (IEGs) (Lyons and West 2011), and mapping IEG
155 expression is a strategy for identifying neuronal populations that are excited by specific stimuli or behavioral
156 contexts (Guzowski et al. 2005). IEG transcripts tend to be recovered at lower levels compared to other genes
157 in sc/snRNA-seq data (Y. E. Wu et al. 2017; Lacar et al. 2016; Moffitt et al. 2018). To better track these signals,
158 we identified genes that were selectively co-transcribed with three established IEGs (*c-fos*, *egr1*, *npas4*)
159 independently across 2° clusters. In total, we identified 25 “IEG-like” genes (Table S6), most (17/25, 68%) of
160 which had previously been identified as IEGs, but eight of which have not (predicted homologues of human
161 *DNAJB5*, *ADGRB1*, *GPR12*, *ITM2C*, *IRS2*, *RTN4RL2*, *RRAD*; Fig. 3A). These genes may include new markers
162 of neuronal excitation.

163 We assigned each nucleus an “IEG score,” equal to the number of unique IEG-like genes expressed. To
164 disentangle building-, quivering-, and GSI-associated signals, we tested a sequence of models in which these
165 variables competed in different combinations to explain variance in IEG score. Effects were considered
166 significant if the raw p-value was significant ($p < 0.05$) in every model and if the FDR-adjusted harmonic mean
167 p-value (hmp_{adj}) was significant across models ($\text{hmp}_{\text{adj}} < 0.05$) (Wilson 2019). Building was associated with
168 increased IEG expression in 9_Glut ($\text{hmp}_{\text{adj}} = 0.0016$; Fig. 3B), a cluster with gene expression patterns reflective
169 of Dd and Dc, two pallial brain regions (Martinelli et al. 2016). We also reasoned that some behaviorally-relevant
170 populations may not align with clusters. For example, neuropeptides can diffuse to modulate distributed cell
171 populations expressing their target receptors (Johnson and Young 2017), and other behaviorally-relevant
172 populations may represent a small proportion of one cluster. We therefore analyzed populations defined by
173 nTF, ligand, and receptor genes, as well as a small set of additional genes of interest ($n=17$, “Other”, Table
174 S5), both within clusters and regardless of cluster. IEG score was associated with building, quivering, and GSI
175 in distinct cell populations (Fig. 3B; Table S6). Building was associated with IEG score in three populations
176 defined regardless of cluster (*elavl4+*, *cckbr+*, *ntrk2+*), and in 4_GABA *htr1d+*, 4_GABA *vjpr2+*, 15_GABA/Glut
177 *tacr2+*, 11_Glut *cckbr+*, and 11.1_Glut *npr2+* nuclei (Fig. 3C), consistent with a role for these molecular systems
178 in the neural coordination of building. Quivering was associated with IEG score in 5.2_GABA *etv1+* nuclei, a
179 subpopulation strongly expressing a suite of dopamine (e.g. *etv1*, *th*, *dat*, *vmat*) and progenitor (e.g. *etv1*, *pax6*)
180 neuron marker genes that are known to be expressed in the olfactory bulb granule cell layer, a region in which
181 new dopaminergic neurons are born in adult teleosts. These data are consistent with previous work showing
182 activation of olfactory and dopaminergic circuitry during courtship in diverse systems (Keleman et al. 2012; van
183 Furth, Wolterink, and van Ree 1995; Ishii and Touhara 2019; Louilot et al. 1991; Johnson and Young 2015).
184 Building- and quivering-associated IEG signals were most strongly associated with behavior expressed
185 approximately 60 minutes prior to sample collection, consistent with previously reported IEG nuclear RNA time
186 courses (Lacar et al. 2016) and further reinforcing their behavioral significance (Fig. 3D).

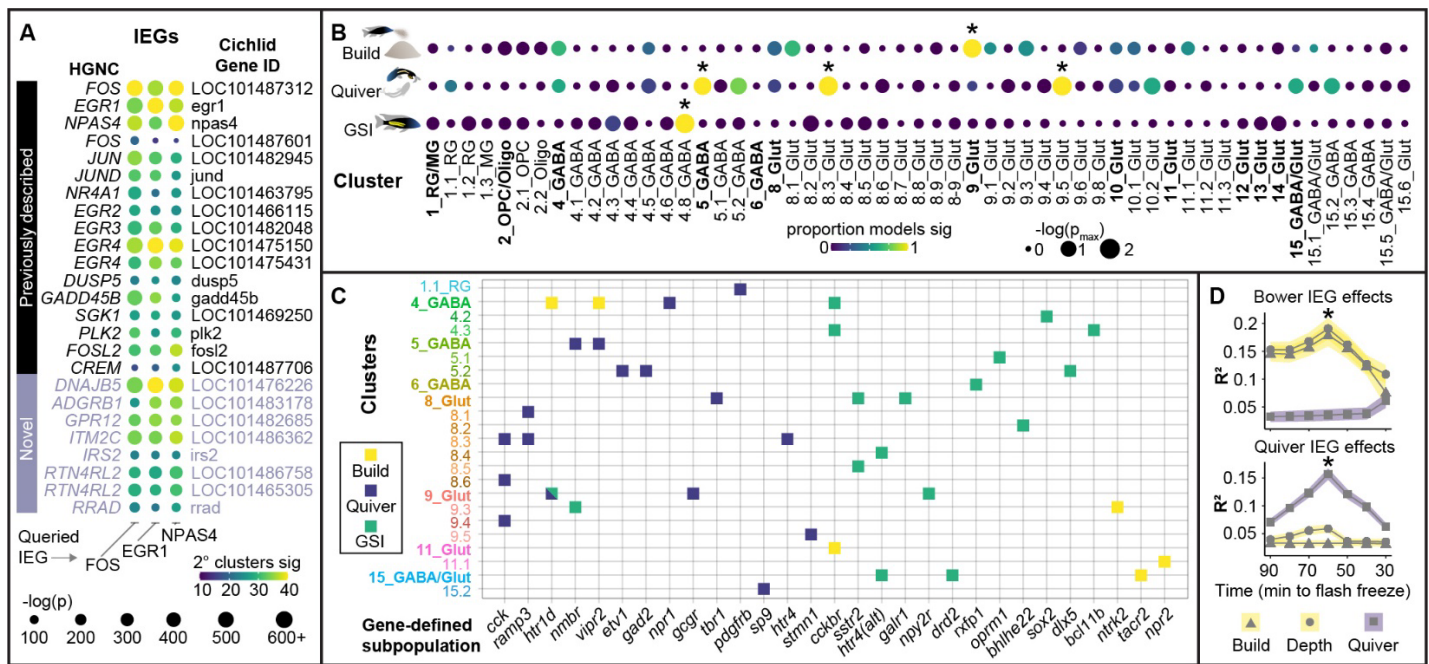


Figure 3. Distinct cell populations exhibit building-, quivering-, and gonadal-associated IEG expression. (A) 25 genes were selectively co-expressed with *c-fos*, *egr1*, and *npas4* across cell populations. (B) Building-, quivering-, and gonadal-associated IEG expression was observed in distinct clusters and (C) gene-defined populations (filled squares indicate significant effects, $q < 0.05$). (D) IEG expression was most strongly associated with the amount of building (top) and quivering (bottom) behavior performed approximately 60 minutes prior to tissue freezing.

A minority of neuronal populations account for the majority of building-associated gene expression

Social behaviors have been linked to large changes in brain gene expression in diverse lineages (Robinson, Fernald, and Clayton 2008; Baran and Streelman 2020; Patil et al. 2021; York et al. 2018), but the underlying cell populations driving these effects are not well understood. We performed an unsupervised analysis to identify differentially expressed genes (DEGs) in specific clusters. A relatively small subset of neuronal clusters accounted for a disproportionate number of building-associated DEGs (bDEGs), a pattern that was also true of quivering-associated DEGs (qDEGs) and gonadal-associated DEGs (gDEGs; Fig. 4A; Table S7). bDEGs were overrepresented in three excitatory neuronal clusters (8_Glut, 9_Glut, 10_Glut; $q \leq 1.83 \times 10^{-4}$ for all), qDEGs were overrepresented in two neuronal clusters (15_GABA/Glut, 11_Glut, $q \leq 0.036$ for both), and gDEGs were overrepresented in one inhibitory neuronal cluster (5_GABA, $q = 1.30 \times 10^{-5}$). bDEGs were overrepresented in a suite of aligned 2° clusters ($q \leq 6.69 \times 10^{-4}$ for all), qDEGs were overrepresented in 15.2_GABA, 8.1_Glut, and 8.6_Glut ($q \leq 0.0074$ for all), and gDEGs were overrepresented in 8.3_Glut and 8.4_Glut ($q \leq 0.039$ for both). Thus, distinct clusters were overrepresented for bDEGs, qDEGs, and gDEGs. Interestingly, despite these non-overlapping signals across clusters, a substantial set of bDEGs, gDEGs, and qDEGs were the same individual genes ($n = 81$), consistent with behavior and gonadal hormones recruiting common transcriptional programs in distinct populations (Fig. 4B). These results highlight a small set of 1° and 2° neuronal clusters as candidate regulators of castle-building behavior.

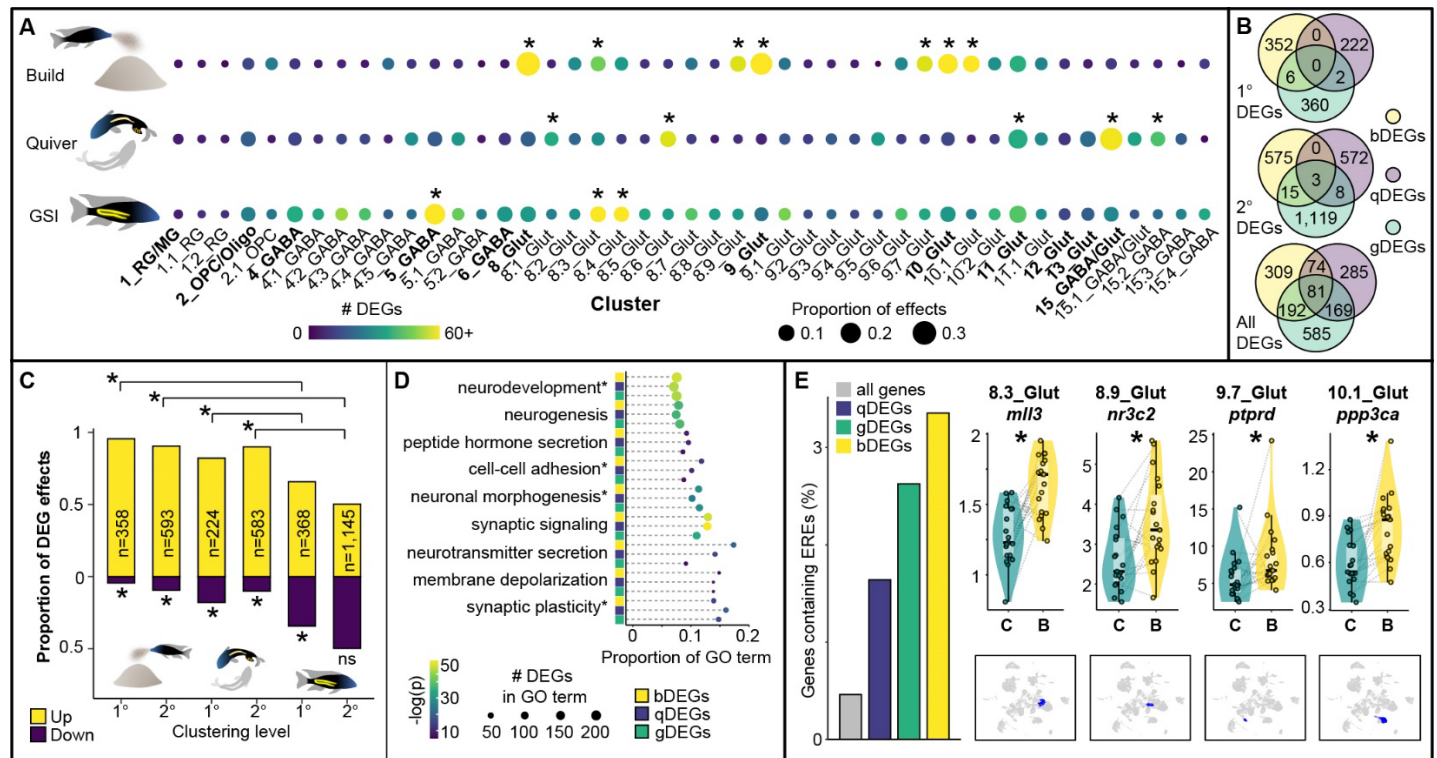
Behavior-associated DEGs exhibited a strong direction bias, and were predominantly upregulated in both 1° and 2° clusters ($p \leq 1.39 \times 10^{-12}$ for all, Fig. 4C). In contrast, gDEGs tended more modestly toward upregulation in 1° clusters (1° gDEG effects, $p = 2.09 \times 10^{-5}$) and were not directionally biased in 2° clusters (2° gDEG effects, $p = 0.92$). Upregulated bDEGs, qDEGs, and gDEGs were each independently enriched for a large number of the same GO terms ($q < 0.05$ for 499 GO Biological Processes, 147 GO Cellular Components, and 111 GO Molecular Functions), the strongest of which were related to synaptic transmission and plasticity (e.g. “synaptic signaling,” $q \leq 3.54 \times 10^{-50}$ for all; “regulation of synaptic plasticity,” $q \leq 1.83 \times 10^{-18}$ for all) or cell differentiation and neurogenesis (e.g. “nervous system development,” $q \leq 6.93 \times 10^{-47}$ for all; “neurogenesis,” $q \leq 4.49 \times 10^{-35}$ for all; “cell morphogenesis involved in neuron differentiation,” $q \leq 6.96 \times 10^{-29}$ for all; Fig. 4D), suggesting behavior- and gonadal-associated regulation of synaptic function and cell morphogenesis.

221
222

Estrogen response elements are enriched in behavior- and gonadal-associated differentially expressed genes

223
224
225
226
227
228
229
230
231
232
233

Estrogen regulates social behavior in diverse species and has been linked to both neuronal excitability and neurogenesis (Diotel et al. 2013; Duarte-Guterman et al. 2015; Kelly and Rønnekleiv 2009; Sarkar et al. 2008). Estrogen can also regulate gene expression by binding to estrogen receptors (ERs), forming a complex that translocates into the nucleus and acts as a TF by binding to Estrogen Response Elements (EREs) in DNA (Klinge 2001; Amenyogbe et al. 2020). bDEGs, qDEGs, and gDEGs were independently enriched for EREs, consistent with a role for estrogen in modulating behavior- and gonadal-associated gene expression ($p \leq 2.92 \times 10^{-4}$ for all; Fig. 4E; ERE-containing gene list in Table S8). ERE-containing bDEGs ($n=22$ unique genes) were most strongly enriched for GO terms including “modulation of chemical synaptic transmission” (top GO Biological Process, $q=2.30 \times 10^{-4}$) and “Schaffer collateral - CA1 synapse” (top Cellular Component, $q=2.22 \times 10^{-5}$), consistent with building-associated estrogenic regulation of synaptic function. These data support a role for estrogen in castle-building behavior.



234

235

Figure 4. Building, quivering, and GSI are associated with distinct patterns of cell type-specific gene expression. (A) Distinct 1° and 2° clusters show a disproportionate number of bDEGs, qDEGs, and gDEGs. (B) A set of 81 genes exhibits building-, quivering, and gonadal-associated expression in largely non-overlapping clusters. (C) Behavior-associated gene expression is driven by upregulation, whereas gonadal-associated gene expression is driven by a balance of up- and downregulation. (D) bDEGs, qDEGs, and gDEGs are enriched for GO terms related to synaptic structure, function, and plasticity; neurotransmission; and neurogenesis. (E) bDEGs, qDEGs, and gDEGs are enriched for EREs. Violin plots show cluster-specific ERE-containing bDEG effects and feature plots below show the clusters (blue) in which each effect was observed. GO terms followed by asterisks are abbreviated.

244

Castle-building is associated with neuronal rebalancing in the putative fish hippocampus

245
246
247
248
249
250

The enrichment of neurogenesis-related GO terms among bDEGs motivated us to further investigate building-associated neurogenesis. During neurogenesis, new neurons differentiate into specific neuronal populations (Mira and Morante 2020; Götz and Huttner 2005), and we therefore reasoned that building-associated neurogenesis may result in build-associated changes in the relative proportions of specific neuronal populations. Analysis of cluster-specific proportions revealed building-associated increases in the relative proportion of 8.4_Glut ($q=0.013$; Fig. 5A,B) and decreases in the relative proportion of 8.1_Glut ($q=7.67 \times 10^{-4}$;

251 Fig. 5A,C). The relative proportions of 8.4_Glut and 8.1_Glut were negatively correlated across subjects, such
252 that greater proportions of 8.4_Glut predicted lesser proportions of 8.1_Glut ($R=-0.50$, $p=0.0012$; Fig. 5D).
253 Notably, 8_Glut was distinguished by markers of the lateral region of the dorsal telencephalon (DI; Table S2),
254 a brain region that is important for spatial learning, memory, and behavior in other fish species. DI is the putative
255 fish homologue of the mammalian hippocampus, a region in which adult neurogenesis regulates spatial
256 learning and memory (Clark et al. 2008; Clelland et al. 2009).

257 **Castle-building is associated with increased expression of genes that positively regulate neurogenesis**

258 To further investigate building-associated neurogenesis, we identified 87 genes with the GO annotation
259 “positive regulation of neurogenesis” in both zebrafish and mice (“proneurogenic” genes, pNGs, Table S9) and
260 analyzed their expression across clusters and gene-defined populations. Building was associated with
261 increased pNG expression in six 1° clusters (8_Glut, 9_Glut, 10_Glut, 11_Glut, 15_GABA/Glut, 4_GABA) and
262 ten aligned 2° clusters (including 8.4_Glut; $hmp_{adj} \leq 0.020$ for all; Fig. 5E). The most significant building-
263 associated pNG expression was observed in 8_Glut (Fig. 5F, $hmp_{adj}=1.23 \times 10^{-17}$), and pNG expression in
264 8.4_Glut specifically was positively associated with its relative proportion ($R=0.33$, $p=0.041$). In contrast to
265 building, gonadal-associated pNG expression was increased in 10.2_Glut ($hmp_{adj}=0.010$) and decreased in
266 4.8_GABA ($hmp_{adj}=0.0048$), and quivering was not associated with pNG expression in any 1° or 2° clusters
267 (Fig. 5E). Notably, the magnitude of effect (β) estimates for building-associated pNG expression in 2° clusters
268 were always greater than in their “parent” 1° clusters, and many gene-defined subpopulations within clusters
269 exhibited stronger building-associated pNG expression than their parent 1° or 2° clusters. For example, within
270 15_GABA/Glut, building-associated pNG estimates were >3x greater in subpopulations defined by expression
271 of *adra2b* ($\beta_{cond}=0.188$) and *esr2* ($\beta_{cond}=0.154$) compared to 15_GABA/Glut as a whole ($\beta_{cond}=0.048$). Among
272 2° clusters, the most extreme cases of this pattern included 8.2_Glut *drd4+*, 8.4_Glut *htr4+*, 9.1_Glut *sstr5+*,
273 9.6_Glut *htr4+*, 10.1_Glut *nrk2+* nuclei, and 11.1_Glut *nrk2+* nuclei ($hmp_{adj} \leq 0.018$ for all). Among populations
274 defined regardless of cluster, those exhibiting building-associated pNG expression were disproportionately
275 defined by neuromodulatory receptor and ligand genes versus nTFs (receptors versus nTFs, $q=0.011$; ligands
276 versus nTFs, $q=0.017$; FET; Fig. 5G), and those exhibiting the strongest building-associated pNG expression
277 (β) effects were disproportionately defined by neuromodulatory receptor genes ($q=0.011$; Fig. 5H), and by ERs
278 in particular ($q=0.034$; Fig. 5I), consistent with a large body of literature supporting relationships between
279 estrogen and neurogenesis (Diotel et al. 2013; Duarte-Guterman et al. 2015). These results highlight specific
280 molecular signaling systems (e.g. estrogen, serotonin, TrkB) that may be involved in building-associated
281 neurogenic changes.

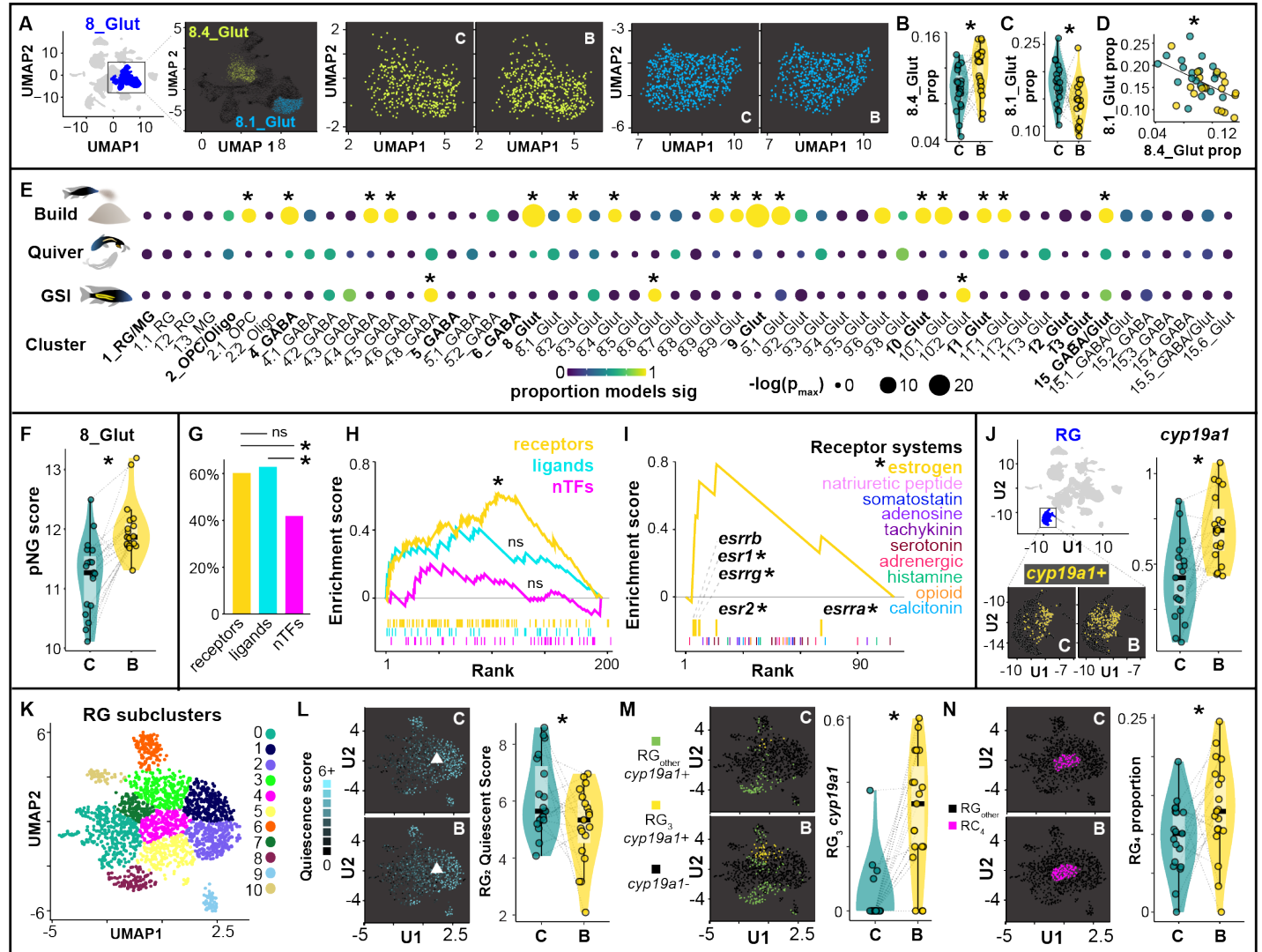
282 **Building is associated with changes in glial cell biology**

283 Radial glia (RG) are the primary source of new neurons in adult teleosts (Ganz and Brand 2016), and we
284 therefore reasoned that signatures of neurogenesis may be downstream effects of changes in RG function. We
285 first investigated building-associated gene expression within radial glia (1.1_RG and 1.2_RG pooled). We
286 identified 25 bDEGs that were collectively enriched for “neuron development” (top GO Biological Process,
287 $q=8.18 \times 10^{-4}$) as well as “astrocytic glutamate-glutamine uptake and metabolism” (top Pathway, $q=0.0010$) and
288 “synapse” (top GO Cellular Component, $q=0.0015$). RG bDEGs included *cyp19a1* (upregulated; Fig. 5J), the
289 gene encoding aromatase, an enzyme that converts testosterone to brain-derived estrogen and has been
290 previously linked to RG function and neurogenesis (Pellegrini et al. 2016).

291 RG can occupy distinct functional states including quiescence, cycling, and neuronal differentiation (Jurisch-
292 Yaksi, Yaksi, and Kizil 2020; Adolf et al. 2006; Labusch et al. 2020). We re-clustered RG (independently of
293 non-RG nuclei) into 11 subclusters (RG₀-RG₁₀; Fig. 5K) and assigned each nucleus a quiescence, cycling, and
294 neuronal differentiation score based on established marker genes (Table S10), and analyzed building-
295 associated differences in these scores across subclusters. Building was associated with decreased quiescence
296 score in RG₂ ($hmp_{adj}=0.010$; Fig. 5L), but was not associated with quiescent, cycling, or neuronal differentiation
297 score in any other subcluster. Analysis of building-associated gene expression across subclusters further
298 revealed that 19/61 subcluster bDEGs were in RG₂, and 18/19 effects reflected building-associated
299 downregulation. The strongest enrichment hit for RG₂ bDEGs was GO Cellular Component “postsynaptic Golgi
300 apparatus” ($q=0.0011$). *cyp19a1* was excluded from analysis in several subclusters because it was not detected
301 in all build-control pairs; however, a targeted analysis revealed that building-associated increases in *cyp19a1*
302 were driven by RG₃ ($hmp_{adj}=0.018$; Fig. 5M), a subpopulation distinguished by *lhx5* and *gli3*, both nTFs that

303
304
305
306
307
308
309

regulate neurogenesis in mammals (Y. Zhao et al. 1999; Hasenpusch-Theil et al. 2018). Lastly, because RG subclusters strongly aligned with functional states, we reasoned that building-associated transitions in RG function may also manifest as building-associated changes in subcluster proportions. Indeed, building was associated with an increase in the relative proportion of RG₄ ($q=0.0017$; Fig. 5N), a subcluster positioned in UMAP space expressing markers of quiescence and nuclei expressing markers of cycling. These data support building-associated changes in radial glial cell biology, and highlight RG₂, RG₃, and RG₄ as candidate RG subpopulations involved in building-associated and RG-mediated neurogenesis.



310

Figure 5. Behavior is associated with signatures of neurogenesis in neurons and glia. (A-C) Building is associated with a shift in the relative proportions in 8.4_Glut and 8.1_Glut, and (D) the relative proportions of these two clusters is strongly correlated across individuals. (E) Building, but not quivering, is associated with increased pNG expression in a large set of 1° and 2° clusters, whereas GSI is associated with increased and decreased pNG expression in just three 2° clusters. (F) The most significant building-associated pNG expression is observed in 8_Glut. (G) Gene-defined populations that exhibit building-associated pNG expression are disproportionately defined by genes encoding receptors and ligands. (H) The strongest building-associated pNG expression tends to occur in populations defined by neuromodulatory receptors, (I) particularly in ER-expressing populations. (J) RG exhibit building-associated *cyp19a1* expression. (K) Reclustered RG subpopulations show building-associated (L) signatures of decreased quiescence (RG₂), (M) *cyp19a1* expression (RG₃), and (N) increases in proportion (RG₄).

322

Genes that have diverged in castle-building lineages are upregulated in reproductive contexts

323
324

Castle-building behavior has previously been linked to a ~19 Mbp region on Linkage Group 11 (LG11), within which genetic variants have diverged between closely-related castle-building and pit-digging lineages (York et

al. 2018; Patil et al. 2021). Our follow up comparative genomics analyses identified 165/756 genes in this region that also showed signatures of divergence between castle-building lineages and more distantly-related “mbuna” species that do not build bowers (“castle-divergent” genes, CDGs; Fig. 6A; Table S11). Thus, CDGs represent a subset of genes bearing strong genomic signatures of castle-building evolution across Lake Malawi species. CDGs were expressed at higher levels in the telencephalon compared to neighboring genes in the same 19Mbp region (~2.9x greater expression, permutation test, $p=1.42 \times 10^{-5}$) and compared to other genes throughout the genome (~2.6x greater expression, $p=1.77 \times 10^{-6}$). CDGs were also overrepresented among 1° and 2° cluster markers (versus neighboring LG11 genes, $p \leq 1.66 \times 10^{-9}$ for both; versus all other genes, $p \leq 1.43 \times 10^{-11}$ for both, FET), and among upregulated bDEGs, qDEGs, and gDEGs (versus neighboring LG11 genes, $p \leq 0.0044$ for all; versus all other genes, $p \leq 0.0066$ for all, FET; Fig. 6B). These data support the behavioral significance of CDGs in the telencephalon, and suggest that castle-building evolution has targeted genes that are selectively upregulated during reproductive contexts.

Castle-divergent genes are enriched in quiescent radial glial subpopulations

CDGs were most strongly enriched in non-neuronal (2.1_OPC, 1.1_RG, and 1.2_RG), followed by neuronal (4.3_GABA and 4.4_GABA) clusters and gene-defined populations (5.2_GABA *th+*, and 9_Glut *hrh3+*; Fig. 6C; Table S12). We hypothesized that co-upregulation of subsets of CDGs in the same nuclei may drive cluster-specific enrichment patterns. A WGCNA (Langfelder and Horvath 2008) based analysis revealed a module of 12 CDGs that were more strongly co-expressed than other CDGs (stronger correlation coefficients, Welch t-test, $p=8.83 \times 10^{-14}$; stronger silhouette widths, Welch t-test, $p=0.016$; Fig. 6D). Across clusters, this module was most strongly enriched in 1.2_RG ($p_{\text{perm}}=0$, Cohen’s $d=4.22$), and was less strongly enriched in 1.1_RG (Cohen’s $d=2.86$; Fig. 6E), suggesting differences in expression among RG subpopulations (Table S13). Within RG, CDG module expression was positively associated with quiescent score (Fig. 6F-H; $R=0.34$, $p=3.21 \times 10^{-52}$; $p_{\text{perm}}=0$); and was negatively associated with cycling score ($R=-0.089$, $p=9.90 \times 10^{-5}$; $p_{\text{perm}}=0$) and neuronal differentiation score ($R=-0.065$, $p=0.0048$; $p_{\text{perm}}=0$). Analysis of co-expression between the module and known TFs ($n=999$) identified *npas3* as an outlier that was most strongly co-expressed TF with the CDG module (Fig. 6I; Table S14; $R=0.47$, $q=3.19 \times 10^{-100}$). *npas3* suppresses proliferation in human glioma, is strongly expressed in quiescent neural stem cells, and is downregulated during hippocampal neurogenesis in mice (Moreira et al. 2011; Shin et al. 2015). Among RG subclusters, the module was selectively enriched in RG₁ ($p_{\text{perm}}=0.0196$) and RG₂ ($p_{\text{perm}}=0.046$; Fig. 6J; Table S13), both of which selectively expressed genetic markers of RG quiescence. Together these data support that CDG module expression is positively related to RG quiescence.

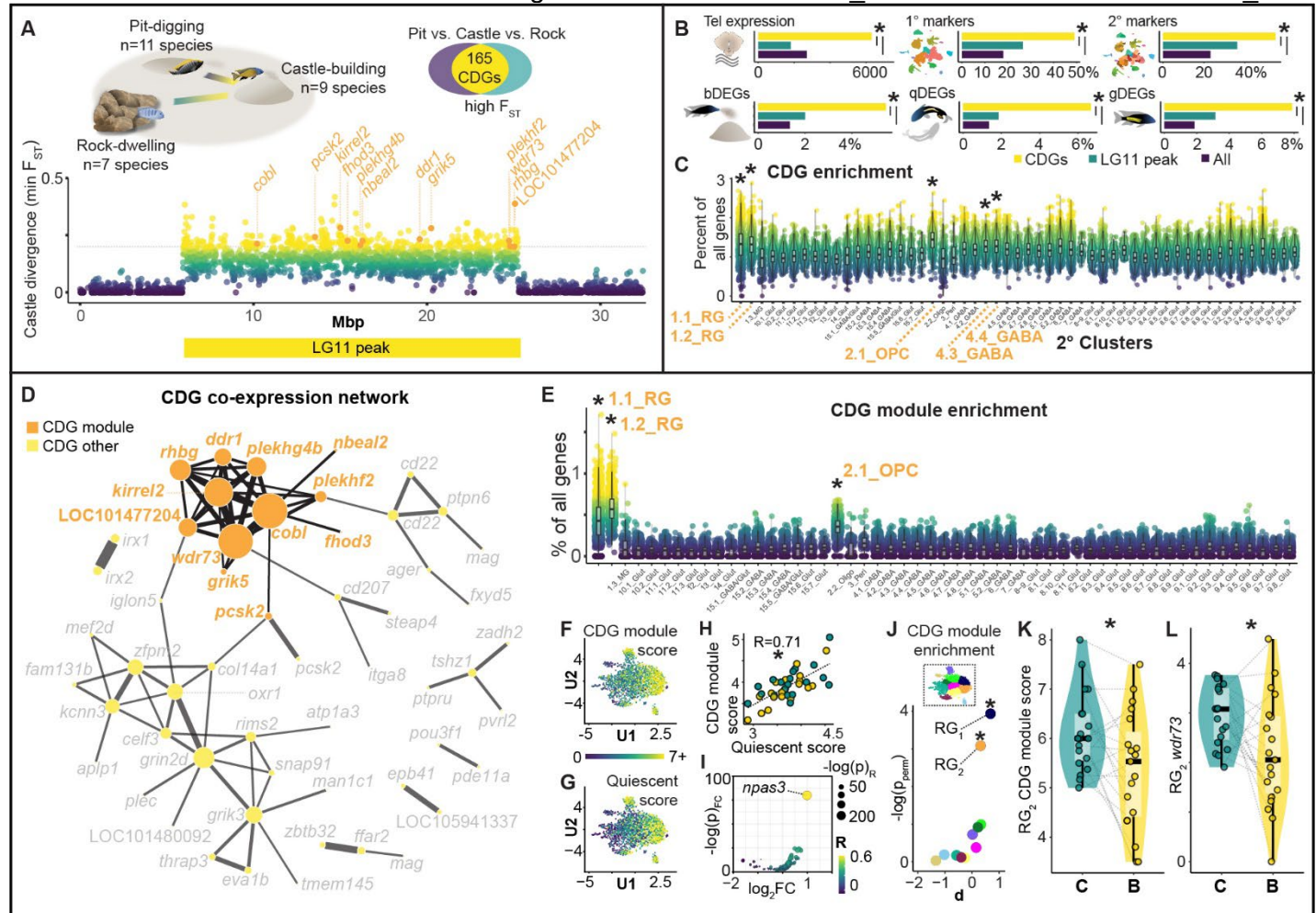
A subpopulation of glia links genome evolution to hippocampal-like neuronal rebalancing

Building was associated with a decrease in CDG module score in RG₂ ($\text{hmp}_{\text{adj}}=0.027$; Fig. 6K), and an increase in CDG module score in RG₈ ($\text{hmp}_{\text{adj}}=0.010$). The only individual CDG module gene for which we detected building-associated expression was *wdr73*, which showed building-associated downregulation in RG₁ and RG₂ ($\text{hmp}_{\text{adj}} \leq 4.54 \times 10^{-89}$ for both; RG₂ effect in Fig. 6L). These data raise the possibility of a building-associated downregulation of the CDG module and an exit from quiescence in RG₂. We hypothesized that a building-associated exit from quiescence in RG₂ may contribute to building-associated neuronal rebalancing between 8.4_Glut and 8.1_Glut. Consistent with this, the 8.4_Glut:8.1_Glut ratio was predicted by RG₂ CDG module score ($R=-0.52$, $p=6.91 \times 10^{-4}$), *wdr73* expression ($R=-0.62$, $p=3.31 \times 10^{-5}$), quiescent score ($R=-0.42$, $p=0.0094$), and *npas3* expression ($R=-0.52$, $p=8.20 \times 10^{-4}$). All of these relationships were evident within building males only (8.4_Glut:8.1_Glut ratio versus RG₂ CDG module score, $R=-0.51$, $p=0.024$; quiescent score, $R=-0.42$, $p=0.059$; versus RG₂ *wdr73* expression, $R=-0.59$, $p=0.0074$; *npas3* expression $R=-0.65$, $p=0.0027$) but not within controls ($p \geq 0.14$ for all). In contrast, none of these relationships were evident in RG₁, regardless of whether the analysis was conducted across all subjects ($p \geq 0.13$ for all) or restricted to building males ($p \geq 0.074$ for all). Together these data are consistent with a role for RG₂ in neuronal rebalancing.

In teleost fishes, anatomically distinct RG subpopulations vary in function and supply new neurons to distinct brain regions (Fig. 7A). We hypothesized that if RG₂ was involved in 8.4_Glut:8.1_Glut neuronal rebalancing, then its anatomical distribution should be consistent with supplying new neurons to brain regions within which 8.4_Glut nuclei reside. Spatial profiling revealed that 8.4_Glut and 8.1_Glut respectively mapped to ventral and dorsal DI-v, a pallial subregion within DI, the putative hippocampal homologue in fish (Fig. 7B-E). Thus, 8.4_Glut and 8.1_Glut both mapped to dorsolateral pallial regions that receive new neurons from RG lining the pallial ventricular zone. RG₂ was anatomically positioned along the pallial but not subpallial ventricular zone

377
378
379

(Fig. 7B-E), consistent with a potential to supply new neurons to DI and other pallial regions. Together these data were consistent with a relationship between building-associated expression of the CDG module in RG₂ and neuronal rebalancing in 8.4_Glut and 8.1_Glut.



380

Figure 6. Genomic signatures of castle-building evolution link behavior, radial glial function, and hippocampal-like neuronal rebalancing. (A) Comparative genomics identifies 165 CDGs (CDG module genes labeled in orange). (B) CDGs are enriched in the telencephalon, among 1° and 2° cluster marker genes, and among bDEGs, qDEGs, and gDEGs. (C) CDGs are most strongly enriched in non-neuronal populations (y-axis shows the percentage of genes expressed that were CDGs). (D) A “CDG module” (orange) contains 12 CDGs that are strongly co-expressed across nuclei. (E) The CDG module is most strongly enriched in radial glia. (F,G) CDG module expression across radial glial subclusters mirrors expression of quiescent markers. (H) Expression of the CDG module is positively correlated with expression of radial glial quiescence markers. (I) *npas3* shows strong, positive, outlier co-expression with the CDG module. (J) RG₁ and RG₂ are enriched for the CDG module. (K) RG₂ exhibits building-associated decreases in expression of the CDG module and *wdr73* in particular (L).

392

Populations excited during building may project to the putative fish hippocampus

393
394
395
396
397
398
399
400
401

In the mammalian hippocampus, the activity of local circuits and incoming projections regulate differentiation of glial cells into new neurons (Pardal and López Barneo 2016; Song et al. 2016). We reasoned that neural activity may similarly regulate building-associated mobilization of RG₂ and neuronal rebalancing. We used CellChat (Jin et al. 2021) to investigate possible connections among 1° clusters, 2° clusters, RG subclusters, and nine gene-defined populations that, in addition to 9_Glut, showed signatures of building-associated excitation (“build-IEG+”; Table S15). Briefly, this tool estimates the molecular potential for connection (“weight”) between cell populations using known cell-cell adhesion and ligand-receptor binding proteins. Unlike most other tools, CellChat increases robustness by additionally accounting for heteromeric complexes and interaction mediator proteins (Dimitrov et al. 2022). As added control, we compared connections between pairs of

402 populations to connections between randomly permuted cell populations of the same size, enabling us to
403 identify connection weights that were greater than 100% of permuted results (Fig. 7F). Weights among neuronal
404 populations of interest (8.1_Glut, 8.4_Glut, and build-IEG+ populations) were greater than weights among other
405 neuronal populations (Fig. 7G; $p=0.03$, Welch two-sample t-test) and among permuted populations (all >100%
406 of permuted connections). Neuronal populations of interest differed in “sending” ($p=0.0016$, Kruskal-Wallis rank
407 sum test) and “receiving” (1.48×10^{-14}) weights, and 8.4_Glut (receiver) had the greatest weights of any sender
408 or receiver (Fig. 7H-I). Compared to other neuronal populations, build-IEG+ populations had greater sending
409 weights to 8.4_Glut ($p=0.027$, Welch two-sample t-test), but not to 8.1_Glut ($p=0.25$; Fig. 7H). These data
410 support a model whereby neuronal populations that fire during building project preferentially to 8.4_Glut
411 neurons.

412 Neuronal firing can increase the strength of synaptic connections. ~2% (64/3,136) of neuronal-neuronal
413 connections exhibited building-associated changes in weight, with building males exhibiting stronger weights
414 in every case. These connections were enriched for build-IEG+ senders (22/64, $p=0.0014$, FET) and 8.4_Glut
415 as a receiver (7/64, $p=1.11 \times 10^{-4}$), but not for build-IEG+ receivers, 8.4_Glut as a sender, or 8.1_Glut as a
416 sender or receiver ($p \geq 0.50$ for all; Fig. 7J). Build-IEG+ sender connections that showed building-associated
417 change were enriched for 8.4_Glut as a receiver (4/22, $p=3.24 \times 10^{-4}$), and 8.4_Glut receiver connections that
418 showed building-associated changes were enriched for build-IEG+ populations as senders (4/7, $p=0.015$).
419 These patterns were driven by senders 9_Glut (Fig. 7K; $\text{hmp}_{\text{adj}}=0.0028$), 4_GABA *htr1d+* (Fig. 7L;
420 $\text{hmp}_{\text{adj}}=0.0081$), 4_GABA *vipr2+* (Fig. 7M; $\text{hmp}_{\text{adj}}=0.0027$), *ntrk2+* ($\text{hmp}_{\text{adj}}=0.011$) and 8.4_Glut (receiver).
421 These data highlight specific populations that may project to DI-v and fire during building.

422 **A behavioral circuit model for activity- and glial-dependent neurogenesis in the putative hippocampus**

423 To investigate relationships among building-associated neural activity, changes in RG biology, and
424 8.4_Glut:8.1_Glut neuronal rebalancing, we used a regularized (LASSO) multiple mediation approach. Briefly,
425 this tested if the relationship between building and 8.4_Glut:8.1_Glut ratio was influenced by any of the following
426 variables: GSI, quivering, all significant RG subcluster and CDG module-related effects (RG₁ *wdr73*, RG₂
427 *wdr73*, RG₂ CDG module score, RG₈ CDG module score, RG₃ *cyp19a1*, RG₄ proportion), IEG score in all ten
428 build-IEG+ populations, and IEG score in 8.1_Glut and 8.4_Glut (Fig. 7N). This analysis revealed RG₂ *wdr73*
429 expression and 4_GABA *htr1d+* IEG score as the only predicted mediators of building-associated neuronal
430 rebalancing (Fig. 7N). To investigate candidate signals that may drive building-associated decreases in RG₂
431 *wdr73* expression, we performed a similar analysis with RG₂ *wdr73* as the outcome. This analysis revealed
432 IEG score in 9_Glut and 4_GABA *vipr2+* as the only predicted mediators of RG₂ *wdr73* expression (Fig. 7N).
433 These data support a model whereby building-associated neural activity in 9_Glut and subpopulations of
434 4_GABA, together with RG₂, coordinate neuronal rebalancing in DI-v. Consistent with this model, spatial
435 integration mapped 9_Glut to the dorsal region of the dorsal telencephalon (Dd) and 4_GABA to
436 dorsal/supracommissural regions of the ventral telencephalon (Vd/Vs; Fig. 7C-E), both of which are
437 reciprocally connected with DI-v in other teleosts (O’Connell and Hofmann 2011b; Giassi, Ellis, and Maler
438 2012).

439 Among populations of interest, connection weights were weakest for RG₂ as a receiver (Fig. 7I), consistent with
440 a lack of direct connections between build IEG+ populations and RG₂. In the mammalian hippocampus, neural
441 activity can regulate glial differentiation into new neurons through “spillover”, or ligand release, diffusion, and
442 binding to target receptors in the absence of direct synaptic connections. We reasoned that a spillover model
443 may be sufficient to explain the data: excitation of 9_Glut, 4_GABA *vipr2+*, and 4_GABA *htr1d+* during building
444 causes secretion of ligands that diffuse and bind to target receptors expressed on nearby RG₂ lining the
445 ventricular zone of DI-v, causing RG₂ to differentiate into new 8.4_Glut neurons. Consistent with this model,
446 examination of ligands expressed in 9_Glut, 4_GABA *vipr2+*, and 4_GABA *htr1d+* and their paired target
447 receptors in RG₂ revealed NRG2-ERBB4 as the top pair (Fig. 7O). *nrg2* was one of 81 bDEGs identified in
448 9_Glut (Fig. 7P), and *erbb4* was preferentially expressed in RG₂ compared to other RG, and in 8.4_Glut
449 compared to 8.1_Glut and compared to other 8_Glut neurons (Fig. 7Q). NRG2-ERBB4 binding promotes both
450 glial cell and neuronal differentiation and, in humans, migration of glioma cells (Ghashghaei et al. 2006;
451 Louhivuori et al. 2018; W.-J. Zhao et al. 2021). Together our data identify a plausible circuit model whereby
452 building-associated neural activity, together with an evolutionarily divergent gene module in glia, coordinate a
453 cellular reorganization of DI-v during building (Fig. 7R).

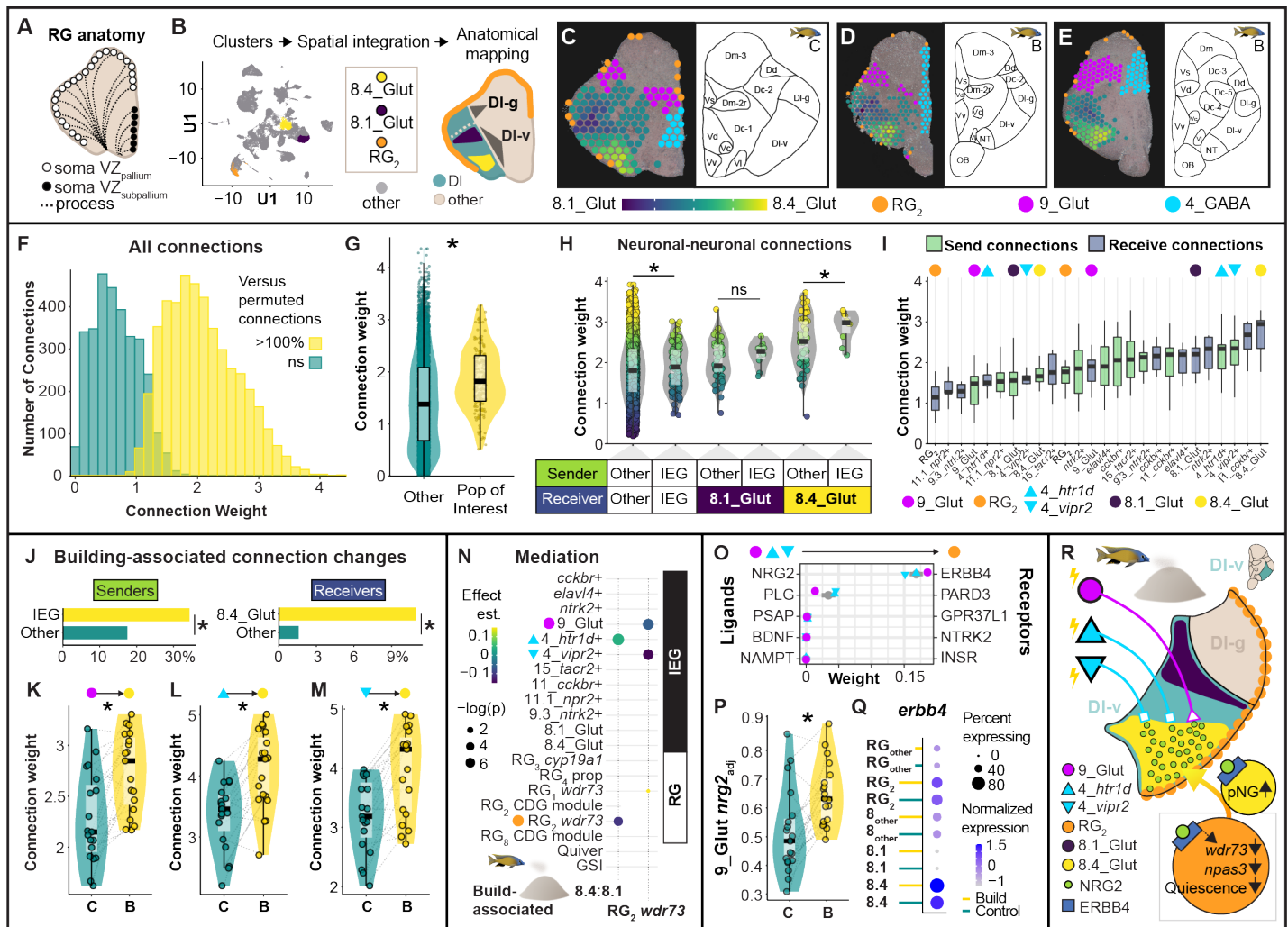


Figure 7. A circuit model for behavior-associated cellular reorganization in hippocampal-like DI-v. (A) RG differ in morphology, function, and anatomical distribution (e.g. pallial versus subpallial ventricular zones). (B) Spatial profiling enables neuroanatomical mapping of RG₂, 8.1_Glut, 8.4_Glut, and additional neuronal populations of interest, as illustrated in three individuals (C-E). RG₂ (orange) aligns with the pallial but not subpallial ventricular zone, and 8.1_Glut versus 8.4_Glut aligns with dorsal versus ventral DI-v, respectively. (F) Cell-cell communication analysis of randomly permuted populations separates bi-modally distributed connections among real populations. (G) Connection weights among populations of interest are stronger than among other populations. (H) Connection weights among build-IEG+ populations are greater than among other neuronal populations, and connection weights and between build-IEG+ populations (senders) and 8.4_Glut (receiver) are greater compared to other neuronal populations (senders) and 8.4_Glut (receiver). (I) Connections to 8.4_Glut (receiver) were greater than any other type of connection among populations of interest. (J) Connections exhibiting building-associated increases in strength were enriched for build-IEG+ senders and for 8.4_Glut as a receiver. (K-M) Connections from 9_Glut, 4_GABA *htr1d*⁺, and 4_GABA *vipr2*⁺ to 8.4_Glut all exhibit building-associated increases in weight. (N) Regularized multiple mediation analysis supports RG₂ *wdr73* expression and 4_GABA *htr1d*⁺ IEG expression as mediators of 8.4_Glut:8.1_Glut neuronal rebalancing, as well as 9_Glut and 4_GABA *vipr2*⁺ IEG expression as mediators of RG₂ *wdr73* expression. (O) NRG2-ERBB4 is the strongest cell-cell molecular signaling pathway identified between 9_Glut, 4_GABA *htr1d*⁺, and 4_GABA *vipr2*⁺ (senders) and RG₂ (receiver). (P) *nrg2* shows building-associated upregulation in 9_Glut. (Q) *erbb4* shows preferential expression in both RG₂ and 8.4_Glut. (R) A circuit model for how neural activity and RG₂ *wdr73* expression may coordinate building-associated neuronal rebalancing in DI-v.

DISCUSSION

454

455

456

457

458

459

460

461

462

463

464

465

466

467

468

469

470

471

472

473

474

475

476

477

478

479 The diversity of social behaviors in nature is an opportunity to discover how conserved genes and cell
480 populations generate variable neural and behavioral responses to social stimuli (Johnson and Young 2018;
481 Jourjine and Hoekstra 2021; Hofmann et al. 2014; O’Connell and Hofmann 2011a). The ability to functionally
482 profile many heterogeneous cell populations in under- and unstudied behavioral and species systems will be a
483 boon to this endeavor. In this study we investigated the neurobiological substrates of castle-building in *Mchenga*
484 *conophoros* by integrating snRNA-seq with comparative genomics and automated behavior analysis. Using
485 natural individual genetic variation, we matched telencephalic nuclei back to 38 test subjects, enabling powerful
486 analyses of building-associated signals that controlled for correlated variables that may explain differences in
487 brain gene expression. We first charted the cellular diversity of the telencephalon, and then profiled behavior-
488 and gonadal-associated gene expression, cell type proportions, genomic signatures of behavioral evolution,
489 and cell-cell signaling systems across telencephalic cell populations. Our results support central and related
490 roles for glia, genome evolution, hippocampal-like neurogenesis, and cell type-specific neural activity in castle-
491 building behavior.

492 **Signatures of neuronal excitation reveal candidate populations activated during building**

493 Different social behaviors are regulated by distinct neural circuits and/or circuit activities in the brain (Newman
494 1999; Goodson 2005; Amadei et al. 2017; Kimchi, Xu, and Dulac 2007; Dulac, O’Connell, and Wu 2014).
495 Identifying which cell populations are important for a specific behavior is difficult, because most tools cannot
496 functionally profile many heterogeneous cell populations at once. Three previous studies have supported the
497 promise of sn/scRNA-seq technologies for mapping behavior-associated IEG expression across many cell
498 populations (Lacar et al. 2016; Moffitt et al. 2018; Y. E. Wu et al. 2017); however, all three studies were
499 conducted in the same genetically inbred C57BL6/J mouse strain, and thus cells that were pooled for
500 sequencing could not be matched back to individual animals. In our study, we leveraged natural genetic
501 variation among individuals to trace ~34,000 nuclei back to 38 individual males and analyzed building-
502 associated IEG expression while accounting for variance explained by other biological and technical factors.
503 Our analysis revealed novel IEG-like genes and distinct patterns of building-, quivering-, and GSI-associated
504 neuronal excitation across clusters and gene-defined cell populations. Building was associated with increased
505 IEG expression in 9_Glut. Spatial profiling mapped 9_Glut to Dd, a pallial region that innervates DI in a many-
506 to-one fashion in other fish, mirroring the conserved “pattern separator” circuit organization within the
507 mammalian hippocampus (Elliott et al. 2017). *ntrk2*+ nuclei also exhibited building-associated IEG expression,
508 highlighting the TrkB system as a candidate player in castle-building. TrkB is a receptor that transduces activity-
509 dependent signals into downstream modulation of neuronal differentiation, morphogenesis, survival, and long
510 term potentiation (LTP) (Badurek et al. 2020; Lipsky and Marini 2007). Interestingly, *ntrk2*+ nuclei also exhibited
511 building-associated pNG expression, suggesting TrkB may link building-associated neuronal firing to building-
512 associated neuronal plasticity. The only other population that exhibited both building-associated IEG and pNG
513 expression was defined by expression of *cckbr* (encodes Cholecystokinin B Receptor). Interestingly, this
514 receptor has recently been linked to NMDA receptor-mediated LTP and hippocampal neurogenesis in mice
515 (Asrican et al. 2020; Chen et al. 2019).

516 **A role for neurogenesis in social behaviors tied to reproductive cycles**

517 Analysis of differential gene expression, pNG expression, cluster proportions, behavior-associated genome
518 divergence, and RG biology supported a role for neurogenesis in the evolution and expression of castle-building
519 behavior. These analyses provided converging evidence for building-associated neurogenesis in 8_Glut, a
520 cluster that anatomically mapped to DI. Briefly, DI is a brain region in the lateral pallium of fish that is thought
521 to be homologous to the mammalian hippocampus based on gene expression, cell morphology, afferent and
522 efferent connectivity, anatomical, and behavioral evidence (Fotowat et al. 2019; Bingman, Salas, and
523 Rodriguez 2008; Rodríguez et al. 2002; O’Connell and Hofmann 2011b; Ganz et al. 2014; Salas et al. 2017;
524 Ocaña et al. 2017). For example, the DI and the hippocampus have demonstrated roles in regulating spatial
525 learning in fish and mammals (including humans), respectively (Engelmann, Wallach, and Maler 2021; Vikbladh
526 et al. 2019; Miller et al. 2018; Nakazawa et al. 2004). Within 8_Glut, building was associated with a shift in the
527 relative proportions of 8.4_Glut and 8.1_Glut, two populations that mapped specifically to ventral DI, a
528 subregion that exhibits selective responses during spatial learning and memory formation in other fish species
529 (Uceda et al. 2015; Ocaña et al. 2017). Our data thus support the possibility that building behavior is associated
530 with a reorganization of hippocampal-like cell populations involved in spatial learning. Interestingly, changes in
531 the social environment induce telencephalic cell proliferation and migration in other cichlid species within three

532 hours, supporting the idea that behavior-associated neurogenesis can occur on relatively short timescales
533 (Maruska, Carpenter, and Fernald 2012).

534 In the wild, bowers are constructed selectively during the breeding season and function as social territories that
535 males aggressively defend against intruders, as well as mating sites for courtship and spawning with females.
536 Bowers are constructed through thousands of spatial decisions about where to scoop and spit sand that
537 ultimately give rise to a species-specific geometric structure. It has been reported in several species that in
538 response to structural damage or destruction (e.g. caused by storms), males will repair or reconstruct the bower
539 to match the size, geometry, and spatial location of the original structure (McKaye, Louda, and Stauffer 1990;
540 Kirchshofer 1953). After the breeding season ends, bowers lose their social significance and are abandoned.
541 Together, these data suggest that spatial learning, memory, and decision-making play a central role in bower-
542 building, and further that spatial representations of the bower are maintained within breeding cycles.
543 Importantly, in our paradigm, control males had previously built, suggesting that the rebalancing was temporary
544 and eventually returned to baseline in the absence of building activity. Within this framework, it is intriguing to
545 speculate that hippocampal-like neuronal rebalancing during building may be related to spatial representations
546 of the bower structure and/or territory. Notably, similar phenomena have been reported in songbirds that repeat
547 their song within a breeding season, but change their song between seasons (Brenowitz and Larson 2015;
548 Goldman and Nottebohm 1983). These birds show robust increases in cell proliferation in vocal learning circuits
549 during the breeding season that decline when the season is over. Neurogenesis may play an important role in
550 seasonal mating behaviors across species, consistent with previous work demonstrating changes in brain
551 region-specific cell proliferation and/or neurogenesis during species-specific social contexts in a variety of taxa
552 (Walton, Pariser, and Nottebohm 2012; Bedos, Portillo, and Paredes 2018; Almlı and Wilczynski 2012;
553 Balthazart and Ball 2016; Maruska, Carpenter, and Fernald 2012; Dunlap, Chung, and Castellano 2013; Lévy
554 et al. 2017). **Estrogenic substrates of male social behavior**

555 Estrogen is a female gonadal steroid hormone that can be synthesized in the male brain via conversion of
556 testosterone to estrogen by aromatase (L. R. Nelson and Bulun 2001). In the brain, estrogen can exert its
557 effects at multiple levels, for example by regulating gene transcription (via EREs), neuronal excitability, synaptic
558 plasticity, neurogenesis, and G-protein coupled receptor signaling (Kelly and Rønnekleiv 2009). Multiple lines
559 of evidence supported a potential role for estrogen in the neural coordination of building. First, bDEGs (as well
560 as qDEGs and gDEGs) contained canonical EREs, consistent with a role for estrogen in modulating building-
561 associated gene transcription. Out of all GO terms, ERE-containing bDEGs were most strongly enriched for
562 “Schaffer collateral - CA1 synapse” (driven by building-associated expression of *cacng2*, *ppp3ca*, *ptprd*, *ptprs*,
563 and *11cam*), a deeply studied hippocampal synapse involved in associative learning and spatial memory in mice
564 (Nakazawa et al. 2004; Soltesz and Losonczy 2018). In mice, estrogen increases the magnitude of long-term
565 potentiation at this synapse (C. C. Smith, Vedder, and McMahon 2009). It is interesting to speculate that
566 estrogen may regulate plasticity in a conserved hippocampal circuit during castle-building behavior. Second,
567 building-associated increases in pNG expression were strongest in populations defined by neuromodulatory
568 receptor genes, and were stronger in populations defined by ERs (*esr1*, *esr2*, *esrra*, *esrrb*, *esrrg*) compared to
569 other receptor families, consistent with previous reports of estrogen-mediated neural plasticity in the
570 mammalian forebrain (Barha and Galea 2010; Brinton 2009; Srivastava and Penzes 2011). Third, building was
571 associated with strong increases in aromatase expression in RG, an effect that was driven most strongly by
572 RG₃. This glial population may coordinate building-associated effects of estrogen on brain gene expression,
573 neural circuit structure and function, and male social behavior, consistent with previous work demonstrating
574 estrogenic regulation of male social behaviors in diverse lineages (M. V. Wu et al. 2009; Huffman, O’Connell,
575 and Hofmann 2013; Sonoko Ogawa et al. 2020; Ervin et al. 2015).

576 **An evolutionarily divergent gene module links neural activity and stem-like glia to hippocampal-like**
577 **neurogenesis and behavior**

578 Glial cells have recently been shown to play central roles in synaptic communication, plasticity, learning,
579 memory, behavior, and psychiatric disease (Santello, Toni, and Volterra 2019; Kastanenka et al. 2020; Nagai
580 et al. 2021; X. Yu et al. 2018). In addition to building-associated aromatase expression in RG, we observed
581 building-associated changes in RG subpopulation-specific gene expression, relative proportions, and
582 signatures of quiescence. Comparative genomic analyses across 26 behaviorally-divergent species further
583 converged on the importance of RG in castle-building behavior, raising the possibility that transcriptional
584 specializations in glia have served as a substrate in castle-building evolution. A module of 12 co-expressed

585 CDGs was tightly linked to signatures of RG quiescence and was enriched in RG₂, a population that showed
586 building- associated downregulation of the CDG module (particularly *wdr73*), *npas3*, and markers of glial
587 quiescence. Interestingly, one study in human epithelial cells found that suppressed *wdr73* expression was
588 most strongly associated with increased expression of *ccnd1* (Tilley et al. 2021), an established marker of
589 proliferation in RG/neural stem cells in vertebrates (Lukaszewicz and Anderson 2011; G. Zhang et al. 2021).
590 Further analysis supported a circuit model whereby behavior-associated neuronal excitation of principal striatal
591 GABAergic (4_GABA *htr1d+* and 4_GABA *vipr2+*) and pallial glutamatergic (9_Glut) projections to 8.4_Glut
592 nuclei in DI-v mediate building-associated decreases in *wdr73* expression in RG₂, which in turn mediates
593 behavior-associated neuronal rebalancing. Examination of molecular ligand-receptor pairs expressed between
594 build-IEG+ populations and RG₂ suggested that a simple spillover model mediated by NRG2-ERBB4 may
595 explain the effect. Our results thus support a model whereby castle-building evolved in part by modifying gene
596 regulatory networks in a glial subpopulation that responds to behavior-associated neural activity and that
597 regulates hippocampal-like neurogenesis. These data are consistent with previous work suggesting that
598 activation of long-range projections into the hippocampus can regulate hippocampal neurogenesis (Káradóttir
599 and Kuo 2018; Song et al. 2016).

600 The CDG module resides in a 19 Mbp genomic region that exhibits signals of divergence mirroring those
601 reported for chromosomal inversions in other species systems (Lamichhaney et al. 2016; da Silva et al. 2019;
602 Tuttle et al. 2016; Corbett-Detig and Hartl 2012; Roesti et al. 2015; Maney et al. 2020; Berg et al. 2017). It is
603 thought that inversions can facilitate rapid evolution by protecting large-scale and adaptive cis-regulatory
604 landscapes and multi-allele haplotypes (“supergenes”) from recombination (Schaal, Haller, and Lotterhos 2022;
605 Hoffmann and Rieseberg 2008; Kirkpatrick and Barton 2006; Villoutreix et al. 2021). Evidence for the
606 importance of inversions in phenotypic evolution has been shown in diverse lineages spanning flowers and
607 humans (Huang and Rieseberg 2020; Stefansson et al. 2005). Two recent studies in the ruff and white-throated
608 sparrows further support that inversions may shape social behavioral evolution in diverse lineages (Merritt et
609 al. 2020; Purcell et al. 2014; Küpper et al. 2016). In our data, four genes in the CDG module, including *wdr73*,
610 are immediately proximate to one end of the 19 Mbp region exhibiting strong behavior-associated divergence.
611 It is therefore intriguing to speculate that these genes reside near an inversion “break point” region with a
612 divergent cis-regulatory architecture in castle-building lineages. Future work is needed to determine if an
613 inversion has shaped cis-regulatory expression of these genes, RG function, and the evolution of castle-
614 building behavior in Lake Malawi cichlid fishes.

615 LIMITATIONS OF THE STUDY

616 The molecular readout in this study was nuclear RNA which may not reflect protein function, for example due
617 to post-transcriptional regulation. Because nuclear RNA can only be captured at a single time point within each
618 individual, temporal analysis of decision-making making behaviors during building was limited. This study only
619 profiled the telencephalon, and other brain regions may play critical roles in castle-building. Lastly, firing
620 properties and circuit connections among populations can be investigated but not proven using snRNA-seq
621 data. Future experiments are required to validate and determine the behavioral roles of specific neural circuits.

622 ACKNOWLEDGEMENTS

623 We thank our collaborators Ashley Parker and Drs. Swantje Graetsch, Manuel Stemmer, and Herwig Baier for
624 valuable feedback during the early stages of the project; Dr. Nicholas Johnson for suggestions regarding
625 statistical analysis of IEG co-expression; Dr. Justin Rhodes for insightful feedback on IEG expression analysis;
626 Cristina Baker for her critical role in initial development of spatial transcriptomics wetlab pipelines; and the
627 Georgia Tech Petit Institute Genome Analysis and Molecular Evolution Cores for their integral roles in sample
628 processing and sequencing, respectively. This work was supported in part by NIH R01GM101095 and
629 R01GM144560 to J.T.S., NIH F32GM128346 to Z.V.J., NIH R35 GM139594 to P.T.M., NSF Graduate
630 Research Fellowship DGE-2039655 to T.J.L., and Human Frontiers Science Program RGP0052/2019 to J.T.S.

631 CONTRIBUTIONS

632
633 General: Z.V.J. initially conceived of the experiment and Z.V.J., J.T.S, and B.E.H. developed and designed it.
634 Z.V.J. and B.E.H. performed all wetlab work (see details below under “Wetlab”). T.J.L. pre-processed
635 behavioral and depth data, including in part spatial and temporal registration of both data streams and temporal

636 anchoring to experimental endpoints. G.W.G. pre-processed snRNA-seq, DNA-seq, and spatial transcriptomics
637 data. Z.V.J. and G.W.G. performed downstream data analysis (see details below under “Drylab”). B.E.H.
638 matched snRNA-seq data to published neuroanatomical expression profiles (see details below under “Drylab”).
639 Z.V.J. took the lead on writing the manuscript with critical feedback from G.W.G., J.T.S., B.E.H., and P.T.M.
640 Z.V.J. took the lead on designing and creating figures with contributions from B.E.H., G.W.G., and T.J.L., and
641 with critical feedback from G.W.G., J.T.S., B.E.H., P.T.M., and T.J.L. J.T.S. mentored and funded Z.V.J.,
642 B.E.H., and G.W.G., and P.T.M. mentored and funded T.J.L. on the project. J.T.S. funded snRNA-seq, DNA-
643 seq, and spatial transcriptomics experiments.

644
645 Wetlab: Z.V.J. and B.E.H. developed and optimized a single nucleus isolation protocol for cichlid telencephala.
646 Z.V.J. and B.E.H. performed all behavioral assays, surgeries, and downstream nuclei isolations for snRNA-
647 seq. Z.V.J. performed DNA isolations for matching nuclei to subjects. B.E.H. performed all behavior assays for
648 spatial transcriptomics. Z.V.J. and B.E.H. performed surgeries for spatial transcriptomics. B.E.H. performed all
649 downstream wetlab work for spatial transcriptomics. The Petit Institute Genome Analysis Core at GT performed
650 library preparation for snRNA-seq, DNA-seq, and spatial transcriptomics. The Petit Institute Molecular Evolution
651 Core at GT performed sequencing for snRNA-seq, DNA-seq, and spatial transcriptomics.

652
653 Drylab: Z.V.J. performed clustering and cluster marker analysis. B.E.H. systematically surveyed the literature
654 to determine conserved neuroanatomical expression patterns of ligand, receptor, nTF, and other cell type-
655 specific marker genes in the teleost telencephalon. B.E.H., G.W.G, and Z.V.J. collaboratively identified markers
656 of RG quiescence, cycling, and neuronal differentiation. Z.V.J. and G.W.G. collaboratively developed many
657 analytical approaches. Z.V.J. conducted behavioral, IEG co-expression, IEG, DEG, pNG, cell proportion, and
658 gene set enrichment (for biological categories) analyses. G.W.G. matched nuclei to subjects and conducted
659 comparative genomics, gene orthologue calling, ERE detection, gene module detection, and cluster enrichment
660 (for gene lists) analyses. G.W.G. performed spatial integration of clusters and B.E.H. matched spatial
661 transcriptomic profiles to brain regions. Z.V.J. and G.W.G. performed cell-cell communication analyses.
662

663 STAR METHODS

664 EXPERIMENTAL MODEL AND SUBJECT DETAILS

665 All cichlids (species *Mchenga conophoros*) used in this study were fertilized and raised into adulthood (>180
666 days) in the Engineered Biosystems Building cichlid aquaculture facilities at the Georgia Institute of Technology
667 in Atlanta, GA in accordance with the Institutional Animal Care and Use Committee guidelines (IACUC protocol
668 number A100029). This colony was originally derived from wild-caught populations collected in Lake Malawi.
669 All experimental animals were collected as fry at approximately 14 days post-fertilization from mouthbrooding
670 females and were raised with broodmates on a ZebTec Active Blue Stand Alone system. At approximately 60
671 days post-fertilization, animals were transferred to 190-L (92 cm long x 46 cm wide x 42 cm tall) glass aquaria
672 and were housed in social communities (20-30 mixed-sex individuals) into adulthood. Environmental conditions
673 of aquaria were similar to those of the Lake Malawi environment; subjects were maintained on a 12-h:12-h
674 light:dark cycle with full lights on between 8am-6pm Eastern Standard Time (EST) and dim lights on for 60
675 minutes between light-dark transition (7am-8am and 6pm-7pm EST) in pH=8.2, 26.7°C water and fed twice
676 daily (Spirulina Flake; Pentair Aquatic Ecosystems, Apopka, FL, U.S.A.). All tanks were maintained on a central
677 recirculating system. Reproductive adult subject males (age 6-14 months post-fertilization, n=38) were visually
678 identified from home tanks based on nuptial coloration and expression of classic courtship behaviors (i.e.
679 chasing/leading, quivering). Reproductive adult stimulus females were visually identified from home tanks
680 based on distension of the abdomen (caused by ovary growth) and/or buccal cavity (caused by mouthbrooding).

681 METHOD DETAILS

682 *Behavior tanks*

683 Behavior tanks were equipped with LED strip lighting synced with external room lighting to minimize large
684 shadows and maximize consistency in video data used for action recognition (10-h:14-h light:dark cycle). Sand
685 (Sahara Sand, 00254, Carib Sea Inc.; ACS00222) was contained within a 38.1 cm long x 45.6 cm wide section
686 of each tank and separated from the rest of the aquarium by a custom 45.6 cm wide x 17.8 cm tall x 0.6 cm
687 thick transparent acrylic barrier secured with plastic coated magnets (1.25 cm wide x 2.5 cm tall x 0.6 cm thick;
688 BX084PC-BLK, K&J Magnetics, Inc.). This design ensured that all fish could freely enter and leave the enclosed
689 sand tray region throughout the trial. At the start of the trial, the smoothed sand surface lay approximately 29.5
690 cm directly below a custom-designed transparent acrylic tank cover (38.1 cm long x 38.1 cm wide x 3.8 cm tall)
691 that directly contacted the water surface to eliminate rippling for top-down depth sensing and video recordings.

692 *Behavior assays*

693 Subject males were introduced to behavioral tanks containing sand and four reproductive adult age- and size-
694 matched stimulus females of the same species. Broods were collected from all mouthbrooding females prior to
695 introduction of subject males to behavior tanks. Prior to behavioral trials, each male was allowed to initiate
696 castle-building to 1) confirm capacity and motivation to build and 2) minimize potential confounding effects of
697 “novelty” on brain gene expression that may be caused by the male’s first experience building. After building
698 was confirmed during the initial “pre-trial” period, the sand surface in each behavioral tank was smoothed
699 shortly before lights off, and an automated depth sensing and video recording protocol was initiated as
700 previously described using a Raspberry Pi 3 mini-computer (Raspberry Pi Foundation) (Johnson, Arrojjwala, et
701 al. 2020). Briefly, this system uses 1) a Microsoft Xbox Kinect Depth sensor to track depth change across the
702 sand surface every five minutes, enabling analysis of the developing bower structure over time, and 2) a
703 Raspberry Pi v2 camera to record 10 hours of high-definition video data daily. The system regularly uploads
704 depth change updates to a Google Documents spreadsheet, enabling real-time, remote monitoring of bower
705 construction activity in each tank. Following each trial, a trained 3D Residual Network was used to predict male
706 building and quivering behaviors from video data as previously described (Long et al. 2020).

707 *Tissue sampling*

708 Actively constructing males (n=19) were identified through remote depth change updates and were collected
709 between 11am-2pm EST (3-5 h after full lights-on and feeding) to control for potential effects of circadian
710 rhythm, feeding, hunger, and anticipation of food on brain gene expression. At the same time, a neighboring
711 male that was not constructing a bower (nor had initiated construction) but could also freely interact with four
712 females and sand, was also collected (“control”, n=19). Immediately following collection, subjects were rapidly
713 anesthetized with tricaine for rapid brain extraction, measured for standard length (SL, distance measured from
714 snout to caudal peduncle) and body mass (BM), and rapidly decapitated for brain extraction. Telencephala
715 (including olfactory bulbs) were dissected under a dissection microscope (Zeiss Stemi DV4 Stereo Microscope
716 8x - 32x, 000000-1018-455), in Hibernate AB Complete nutrient medium (HAB; with 2% B27 and 0.5 mM
717 Glutamax; BrainBits) containing 0.2 U/μl RNase Inhibitor (Sigma). Immediately following dissection
718 telencephala were rapidly frozen on powdered dry ice and stored at -80 °C. Testes were then surgically
719 extracted and weighed to calculate gonadosomatic index (GSI=gonad mass/BM*100) for each subject (subject
720 information available in Table S1).

721 *Nuclei isolation*

722 Nuclei were isolated following a protocol adapted from (Martelotto 2020) and optimized for cichlid telencephala.
723 Immediately prior to single nuclei isolation, frozen telencephala were pooled into five biological replicates (n=3-
724 4 subjects/pool) per behavioral condition (building versus control). Pools were organized such that individuals
725 within a pool had nearly identical telencephalic mass with the aim of equalizing the relative mass of tissue and
726 the relative number of nuclei sampled from each subject within each pool. Additionally, paired constructing
727 versus control pools were organized such that males in both pools were matched as closely as possible in
728 relative age, body mass, and sampling dates. Frozen telencephalon tissue sample pools were transferred into
729 chilled lysis buffer containing 10 mM Tris-HCL (Sigma), 10 mM NaCl (Sigma), 3 mM MgCl₂ (Sigma), 0.1%
730 Nonidet P40 Substitute (Sigma), and Nuclease-free H₂O. The tissue was incubated on ice and lysed for 30
731 minutes with gentle rotation. Following lysis, 1.0 mL HAB medium was added and the tissue was rapidly
732 triturated 20 rounds using silanized glass Pasteur pipettes (BrainBits) with a 500 μm internal diameter to
733 complete tissue dissociation. Dissociated tissue were centrifuged (600 rcf, 5 minutes, 4°C) and resuspended
734 in 2.0 ml chilled wash and resuspension buffer containing 2% BSA (Sigma) and 0.2 U/μl RNase Inhibitor
735 (Sigma, as described above “Tissue Collection”) in 1X PBS (Thermo Fisher). The nuclei suspensions were
736 filtered through 40 μm Flowmi[®] cell strainers (Sigma) and 30 μm MACS[®] SmartStrainers (Miltenyi) to remove
737 large debris and aggregations of nuclei prior to fluorescence activated cell sorting (FACS).

738 *Fluorescence Activated Cell Sorting*

739 Pilot experiments revealed that multipllets (clumps of multiple nuclei adhered together) passed through both
740 passive filtration steps, and therefore we further improved the quality and purity of our sample using FACS (BD
741 FACSaria[™] Fusion Cell Sorter, BD Biosciences). Sizing beads (6 μm; BD Biosciences) and 1.0 μg/ml DAPI
742 (Sigma) were used to set gating parameters, enabling selection of singlet nuclei based on size (forward scatter),
743 shape (side scatter), and DNA content (DAPI fluorescence). Thus, this step efficiently filtered out multipllets and
744 irregularly shaped nuclei (characteristic of unhealthy or dead nuclei). At least 300,000 nuclei/pool were
745 collected into 1 mL wash and resuspension buffer for downstream sequencing.

746 *snRNA-sequencing*

747 Suspensions of isolated nuclei were loaded onto the 10x Genomics Chromium Controller (10x Genomics) at
748 concentrations ranging from 400-500 nuclei/ul with a target range of 3,000–4,000 nuclei per sample.
749 Downstream cDNA synthesis and library preparation using Single Cell 3' GEM, Library and Gel Bead Kit v3.1
750 and Chromium i7 Multiplex Kit were performed according to manufacturer instructions (Chromium Single Cell
751 3' Reagent Kits User Guide v3.1 Chemistry, 10X Genomics). Sample quality was assessed using high
752 sensitivity DNA analysis on the Bioanalyzer 2100 system (Agilent) and libraries were quantified using a Qubit
753 2.0 (Invitrogen). Barcoded cDNA libraries were pooled and sequenced on the NovaSeq 6000 platform (Illumina)
754 on a single flow cell using the 300-cycle S4 Reagent kit (2x150 bp paired-end reads; Illumina).

755 *DNA sequencing*

756 Genomic DNA was isolated from diencephalic tissue sampled from each test subject using a DNeasy Blood
757 and Tissue Kit pipeline with a 60 min lysis time and without RNase A. The 260/280 nm absorbance ratio ranged
758 from 1.91-2.10 across subjects. Libraries were prepared following a NEBNext Ultra II FS DNA Library Prep Kit
759 for Illumina protocol. Libraries were sequenced on two NovaSeq 6000 lanes using 300-cycle SP Reagent Kits
760 (2x150 bp paired-end reads; Illumina).

761 *Spatial transcriptomics*

762 Telencephala were microdissected from two size-matched build-control pairs of *Mchenga conophoros* males
763 (n=4 males total), embedded in cryomolds, flash frozen on dry ice, and stored at -80°C until further processing.
764 Tissue was cryo-sectioned coronally at 10-µm thickness at -20°C (Cryostar NX70) and mounted onto pre-
765 chilled Visium Spatial Gene Expression slides (10X Genomics). RNA quality (RIN > 7) was confirmed using an
766 RNA 6000 Nano Kit (Agilent). Spatial gene expression slides were processed following manufacturer
767 instructions (Visium Spatial Gene Expression Reagent Kits User Guide, 10X Genomics). Barcoded cDNA
768 libraries were sequenced on the NovaSeq 6000 platform (Illumina).

769 **QUANTIFICATION AND STATISTICAL ANALYSIS**

770 *Behavioral Analysis*

771 For all trials, 3D ResNet-predicted behaviors and structural change across the sand surface was analyzed over
772 the 90 minutes preceding collection following the same general approach described previously ([Johnson,
773 Arrojwala, et al. 2020](#)). Briefly, a smoothing algorithm was applied to remove depth change attributable to
774 technical noise, and small regions of missing data were recovered by spatial interpolation. Bowers were defined
775 as any region within which one-thousand or more contiguous pixels (equivalent to ~10 cm²) changed in
776 elevation by more than 0.2 cm in the same direction (~2 cm³ volume change total) based on previous analysis
777 of depth change caused by non-building home tank activity ([Johnson, Arrojwala, et al. 2020](#)). Depth change
778 values were adjusted based on the cubed standard length of each subject male, to create a standardized
779 measure of building activity (larger males have larger mouths and can scoop and spit a larger volume of sand).
780 Action recognition was used to track the number, location, and timepoints of predicted bower construction
781 behaviors (scoops, spits, and multiple events) and quivering behaviors over the same 90 min period. The
782 number of quivering events was log-normalized due to a single outlier (building) male with 257 predicted
783 quivering events (~5.9 standard deviations above the mean). Feeding behaviors were not analyzed because
784 they can be performed by both males and females and we are not able to reliably attribute individual feeding
785 events to the subject male.

786 For simplicity, we generated a single “Bower Activity Index” (BAI) metric to reflect overall building activity by
787 first calculating the regression line between depth change and building events for each trial (n=38, R²=0.76).
788 We then projected each male’s depth change and bower behavior values onto that line, with the lowest value
789 (0 predicted building events, 0 above threshold depth change) being set to 0. BAI was calculated as the
790 Euclidean distance along the regression line from the lowest value. BAI was used as a continuous measure of
791 castle-building behavior throughout this study.

792 Differences in building, quivering, and GSI between groups were analyzed using a paired t-test in which behave
793 and control subjects collected at the same time were treated as pairs.

794 *snRNA-seq pre-processing and quality control*

795 FASTQ files were processed with Cell Ranger version 3.1.0 (10X Genomics). Reads were aligned to the
796 *Maylandia zebra* Lake Malawi cichlid genome assembly (Conte et al. 2019) using a splice-aware alignment
797 algorithm (STAR) within Cell Ranger, and gene annotations were obtained from the same assembly (NCBI
798 RefSeq assembly accession: GCF_000238955.4, M_zebra_UMD2a). Because nuclear RNA contains intronic
799 sequence, they were included in the cellranger count step. Cell Ranger filtered out UMIs that were
800 homopolymers, contained N, or contained any base with a quality score less than 10. Following these steps,
801 Cell Ranger generated ten filtered feature-barcode matrices (one per pool) containing expression data for a

802 total of 32,471 features (corresponding to annotated genes) and a total of 33,895 barcodes (corresponding to
803 droplets and putative nuclei) that were used passed through additional quality control steps in the “Seurat”
804 package in R. Examination of total transcripts, total genes, and proportion of mitochondrial transcripts were
805 similar across all ten pools, and therefore the same criteria were used to remove potentially dead or dying
806 nuclei from all pools. Barcodes associated with fewer than 300 total genes, fewer than 500 total transcripts, or
807 greater than 5% (of total transcripts) mitochondrial genes were excluded from downstream analysis on this
808 basis. This step filtered out a total of 20 (0.059%) barcodes. To reduce risk of doublets or multiplets, barcodes
809 associated with more than 3,000 total genes or 8,000 total transcripts were also excluded. This step filtered out
810 a total of 201 barcodes (0.59%). In total, 33,674 barcodes (99.34%) passed all quality control filters and were
811 included in downstream analyses.

812 *Dimensionality reduction*

813 In order to perform dimensionality reduction, we first identified 4,000 genes that exhibited the most variable
814 expression patterns across nuclei using the FindVariableFeatures function in Seurat with the mean.var.plot
815 selection method, which aims to identify variable features while controlling for the strong relationship between
816 variability and average expression, and otherwise default parameters. Gene-level data was then scaled using
817 the ScaleData function in Seurat with default parameters. To examine dimensionality, we first performed a
818 linear dimensional reduction using the RunPCA command with the maximum possible number of dimensions
819 (“dim” set to 50). We then used Seurat’s JackStraw, ScoreJackStraw, and JackStrawPlot functions to estimate
820 and visualize the significance of the first 50 principal components (PCs), and the Elbow plot function to visualize
821 the variance explained by the first 50 PCs. Because all 50 PCs were highly statistically significant, and no “drop
822 off” was observed in variance explained across PCs, we used all 50 PCs for non-linear dimensional reduction
823 (Uniform Manifold Approximation and Projection, UMAP) using the RunUMAP function in Seurat. For
824 RunUMAP, “min.dist” was set to 0.5, “n.neighbors” was set to 50, and “metric” was set to “euclidean”.

825 *Clustering*

826 Prior to clustering, nuclei were embedded into a K nearest-neighbor (KNN) graph based on euclidean distance
827 in UMAP space, with edge weights based on local Jaccard similarity, using the FindNeighbors function in Seurat
828 (k.param=50, dims=1:2, prune.SNN=0). Clustering was then performed using Seurat’s FindClusters function
829 using the Louvain algorithm with multilevel refinement (algorithm=2). This final step was performed twice using
830 two different resolution parameters to generate both coarse- and fine-grained structural descriptions of the
831 underlying data, facilitating investigation of both major cell types as well as smaller subpopulations. For more
832 coarse-grained clustering (resolution=0.01) identified 15 1° clusters and fine-grained clustering (resolution=1.3)
833 identified 53 2° clusters.

834 *Cluster marker gene analysis*

835 The biological identities of specific clusters were investigated using a multi-pronged approach that incorporated
836 unbiased analysis of cluster-specific marker genes as well as supervised examination of previously established
837 marker genes. Cluster-specific “marker” genes were identified using the FindAllMarkers function in Seurat.
838 Briefly, this function compares gene expression within each cluster to gene expression across all other clusters
839 and calculates Bonferroni-adjusted p-values using a Wilcoxon rank sum test. Functional enrichment analysis
840 of GO categories among cluster-specific marker genes was investigated by first converting cichlid gene names
841 to their human orthologs and then performing functional enrichment analysis using ToppGene Suite with default
842 parameters. Enrichment results that survived FDR-adjustment ($q < 0.05$) were considered statistically
843 significant. Established cell type-specific and neuroanatomical marker genes were identified from the literature
844 (Table S2) and were intersected with the output from FindAllMarkers to generate further insight into the
845 biological identity of clusters.

846 *Assignment of nuclei to test subjects*

847 To match individual nuclei to individual test subjects, we used Demuxlet to match variants identified in snRNA-
848 seq reads to variants identified from genomic sequencing of each subject (Kang et al. 2018). First, genomic
849 DNA from every test subject was collected and sequenced. In total, 276.7 Gbp of sequenced reads were

850 assigned quality scores ≥ 30 (91.4% of all reads). The corresponding FASTQ files were filtered and aligned to
851 the *M. zebra* Lake Malawi cichlid genome umd2a assembly (NCBI RefSeq assembly accession:
852 GCF_000238955.4, *M_zebra_UMD2a*). The resulting bam file was sorted, duplicates removed, read groups
853 added, and indexed using Picard tools. Variants were then called using GATK v4.1.8.1 HaplotypeCaller using
854 the *M. zebra* umd2a reference genome. Based on pool, individual vcf files were merged, resulting in 10 files
855 (one for each pool). These files were then filtered to retain only variants that varied among individuals in a pool.
856 For each pool, only SNPs for which 1) at least one individual from the pool had a different genotype from the
857 other individuals, and 2) no individuals had missing data, were used as input to Demuxlet. The number of SNPs
858 used ranged from 112,385 to 357,177 with a mean of $241,780 \pm 22,369$ per pool.

859 Next, variants were called from snRNA-seq reads following a similar pipeline. Reads from Cell Ranger's output
860 bam file were filtered for those that passed the quality control metrics described above using samtools v1.11.
861 The resulting bam file was sorted, duplicates removed, read groups added, and indexed using Picard tools.
862 Variants were then called using GATK HaplotypeCaller using the *M. zebra* umd2a reference genome and
863 without the MappingQualityAvailableReadFilter to retain reads that were confidently mapped by Cell Ranger
864 (MAPQ score of 255). The SNPs from the snRNA-seq reads and the genomic DNA were input to Demuxlet,
865 which computed a likelihood estimation that each nucleus belongs to each individual in the pool. Nuclei were
866 assigned to the individual test subject with the greatest probability estimated by Demuxlet.

867 *Identification of IEG-like genes*

868 Three canonical IEGs (*c-fos*, *egr1*, *npas4*) were used to identify additional genes exhibited IEG-like expression
869 across clusters. For each of these three IEGs, nuclei were split into IEG-positive versus IEG-negative nuclei
870 within each of the 53 clusters. Within each cluster, differential gene expression was analyzed between IEG-
871 positive versus IEG-negative nuclei using the FindMarkers function in Seurat, with "logfc.threshold" set to 0,
872 and "min.pct" set to 1/57 (57 was selected as this was the number of nuclei in the smallest cluster). Within each
873 cluster, any genes that did not meet this criterion were excluded and were assigned a p-value of 1. Because
874 FindMarkers requires at least three nuclei to be present in both comparison groups, clusters that contained
875 less than three IEG-positive nuclei were excluded. Genes that were detected in the majority of clusters, and
876 that were significantly ($p < 0.05$) upregulated in IEG-positive nuclei in the majority of those clusters were
877 considered to be significantly co-expressed with each individual IEG. Genes that were significantly co-
878 expressed with all three IEGs were used as IEG-like markers for downstream analyses of IEG-like expression.

879 *Differential IEG expression*

880 Building-, quivering-, and gonadal-associated IEG expression was analyzed in 1° and 2° clusters, gene-defined
881 populations within 1° and 2° clusters, and gene-defined populations regardless of cluster. To do this, we
882 calculated an IEG score for each nucleus, equal to the number of unique IEG-like genes ($n=25$) expressed.
883 Building-, quivering-, and gonadal-associated differences in IEG score were analyzed using a beta-binomial
884 model in which the number of IEG-like genes observed as well as the number of the IEG-like genes not
885 observed were tracked as indicators of recent neuronal excitation. This analysis was performed using the
886 'BBmm' package in R ($m=25$). Because castle-building, quivering, and GSI were correlated with one another,
887 we analyzed expression using a sequence of beta-binomial mixed-effects models in which different pairwise
888 combinations of predictor variables (building, quivering, and GSI) competed to explain variance in IEG score.
889 These models also included nested random terms to account for variance explained by individual variation,
890 pair, pool, and RNA isolation/cDNA library generation batch. Within this framework, we ran the following seven
891 models, which allowed building (analyzed as either a binary or a continuous variable), quivering, and GSI to
892 compete in all possible combinations to explain variance in IEG score:

- 893
- 894 1. IEG score \sim **BAI** + **log(quivering events)** + (*subject/pool/batch*) + (*subject/pair*)
- 895 2. IEG score \sim **BAI** + **GSI** + (*subject/pool/batch*) + (*subject/pair*)
- 896 3. IEG score \sim **BAI** + **log(quivering events)** + **GSI** + (*subject/pool/batch*) + (*subject/pair*)
- 897 4. IEG score \sim **Condition** + **log(quivering events)** + (*subject/pool/batch*) + (*subject/pair*)
- 898 5. IEG score \sim **Condition** + **GSI** + (*subject/pool/batch*) + (*subject/pair*)
- 899 6. IEG score \sim **Condition** + **log(quivering events)** + **GSI** + (*subject/pool/batch*) + (*subject/pair*)
- 900 7. IEG score \sim **log(quivering events)** + **GSI** + (*subject/pool/batch*) + (*subject/pair*)

901

902 We defined significant building-, quivering-, and gonadal-associated IEG effects as those in which 1) the raw
903 p-value for the corresponding fixed effect (for building, BAI and condition; for quivering, log-normalized
904 quivering; for gonadal, GSI) was significant ($p < 0.05$) in every model, and 2) the harmonic mean p-value across
905 models was significant after adjusting for multiple comparisons for all genes and populations analyzed
906 ($\text{hmp}_{\text{adj}} < 0.05$). To calculate the harmonic mean p-value, we used the “harmonicmeanp” package in R. Thus,
907 building-associated IEG effects were significant (the raw p-value for the effect of “condition” and “BAI” < 0.05)
908 in models 1-6, and if the harmonic mean p-value across models 1-6 was significant after adjusting for multiple
909 comparisons across all cell populations.

910 *Building-, quivering-, and gonadal-associated gene expression*

911 Building-, quivering-, and gonadal-associated gene expression was analyzed within 1° and 2° clusters using a
912 multiple linear mixed-effects regression approach with the “glmmSeq” package in R
913 (<https://github.com/KatrionaGoldmann/glmmSeq>). Because castle-building, quivering, and GSI were correlated
914 with one another, we analyzed expression using a sequence of linear mixed-effects regression models in which
915 different pairwise combinations of predictor variables (building, quivering, and GSI) competed to explain
916 variance in gene expression. These models also included nested random terms to account for variance
917 explained by individual variation, pair, sample pool, and 10X Chromium run. Thus, sample size was equal to
918 the number of individuals ($n=38$), with many repeated observations being recorded from each individual (equal
919 to the number of nuclei sampled from that individual as assigned to the cluster being analyzed). Building was
920 analyzed both as a continuous variable (BAI) and as a binary categorical variable (behave versus control).

921

922 We defined bDEGS, qDEGs, and gDEGs as genes (within clusters) in which expression was significantly (raw
923 $p < 0.05$) associated with the corresponding fixed effect (for bDEGs, BAI and condition; for qDEGs, log-
924 normalized quivering; for gDEGs, GSI) in every model, and additionally in which the harmonic mean p-value
925 across models was significant after adjusting for multiple comparisons for all genes and all clusters (5% false
926 discovery rate). For each model, dispersion was estimated for each gene using the “DESeq2” package in R,
927 using parameters recommended for single cell datasets ($\text{fitType} = \text{“glmGamPoi”}$, $\text{minmu} = 1\text{e-}06$). Size factors
928 for each gene were calculated using the “scran” package in R, using default parameters, except that
929 max.cluster.size was set to the number of nuclei assigned to the cluster being analyzed. Genes that were not
930 observed in 19/19 pairs were excluded from analysis.

931 *Estrogen response element detection*

932 Estrogen receptors are hormone-dependent transcription factors capable of regulating target gene expression
933 by binding to specific DNA sequences called estrogen response elements (EREs). EREs can be easily
934 identified by their prototypic motif of AGGTCA separated by a 3-base spacer ([Ikeda, Horie-Inoue, and Inoue
935 2015](#)). Genes with an ERE motif less than 25 kilobases away were found and the location of the ERE relative
936 to the gene was recorded as either intragenic (ERE within the start site to the 3' polyA tail), promoter (ERE \leq
937 5 kb upstream of the gene), or distal (all other locations less than 25 kb away from the gene). To identify the
938 location of the ERE to the closest gene, bedtools v2.29.1 was used using the closest command.

939 *Building-, quivering-, and gonadal-associated pNG expression*

940 Building-, quivering-, and gonadal-associated pNG expression was analyzed in 1° and 2° clusters, gene-
941 defined populations within 1° and 2° clusters, and gene-defined populations regardless of cluster using the
942 same general approach described for IEG expression, except that building-associated effects were defined as
943 those that were significantly associated with condition in all models. Because we did not expect neurogenesis
944 or associated cellular processes to proceed over 90-minute timescales, we did not additionally require effects
945 to be significantly associated with BAI in all models.

946 *Building-associated changes in cell proportions*

947 Behavior-associated differences in cell type-specific proportions were analyzed for 1° and 2° clusters with a
948 binomial mixed-effects regression model using the glmer function within the “lmer” package in R. The model

949 included condition, GSI, and quivering as fixed effects, and included a random term for individual variation. 1°
950 cluster proportions were calculated as the proportion of all nuclei assigned to each 1° cluster, and 2° cluster
951 proportions were calculated as the proportion of 1° “parent” cluster nuclei assigned to each 2° “daughter”
952 cluster. Thus, each nucleus was treated as an observation with a binary outcome (either an instance of the
953 target cluster or not) from an individual that could be explained by condition, quivering, or GSI. p-values were
954 estimated using the ‘lmerTest’ package in R, and q-values were calculated using the ‘qvalue’ package in R.
955 Building-associated effects were defined as those that were significant after accounting for multiple
956 comparisons across all clusters with a false discovery rate of 5% ($q < 0.05$).

957 *Cluster-specific enrichment of gene sets*

958 To test if genes associated with the evolution of bower construction behavior (identified through comparative
959 genomics) were enriched in specific cell populations, we first calculated a “gene set score” for each nucleus,
960 equal to the total number of unique behavioral evolution genes expressed. Because the gene set score could
961 be impacted by the total volume of sequence data sampled from each nucleus, we divided the gene set score
962 by the total number of unique genes expressed in each nucleus. To quantify enrichment, a Z-test was then
963 used to compare “normalized” gene set scores for all nuclei within a cluster compared to all other nuclei. The
964 distribution of the normalized values was assumed to be normal according to the central limit theorem and
965 population standard deviation was approximated using sample standard deviation.

966 Secondly, the effect size, as measured by Cohen's d, of the results were compared to those of random gene
967 lists. To prevent differences in overall amount of expression between random genes and genes of interest from
968 skewing results, random genes lists were chosen that had approximately equal number of UMIs expressed as
969 a whole to the genes of interest. This was achieved by first ranking all the genes from the highest number of
970 UMIs expressed to the lowest. Next, for each gene of interest, a pool of 100 random genes were chosen that
971 were ranked most closely to the gene of interest and were not a gene of interest themselves. Then, 10,000
972 random gene lists were created by choosing one gene at random from each pool. The enrichment test
973 described above was then performed on the random gene lists. Finally, clusters that were significantly enriched
974 for the genes of interest according to the process above and had significantly greater effect sizes than the
975 10,000 random gene lists were considered to be significant.

976 *RG subclustering*

977 RG subclusters were determined using the same general procedure used for clustering 1° and 2° clusters but
978 restricted to only those nuclei assigned to 1.1_RG and 1.2_RG.

979 *Analysis of castle-associated genomic divergence*

980 In order to identify potential behavior-associated genomic variants, comparative genomic analyses were
981 performed using genomic sequence data collected from 27 Lake Malawi cichlid species (Patil et al. 2021).
982 Fixation indices (F_{ST}) were calculated for polymorphic variants in two separate analyses using vcfTools v0.1.17.
983 The first analysis compared pit-digging (N=11) versus castle-building (N=9) species, and the second compared
984 rock-dwelling (N=7) versus castle-building (N=9) species. Variants for which sequence data was missing from
985 50% or more of species in either group were excluded from analysis. F_{ST} analyses were performed separately
986 using the --weir-fst-pop and --fst-window-size 10000 flag to calculate F_{ST} across 10kb bins in vcfTools. Then,
987 bins where F_{ST} was greater than 0.20 in the pit-castle comparison and 0.20 in the rock-castle comparison were
988 kept. These thresholds are both greater than the minimum F_{ST} of FDR-adjusted significant bins. By creating
989 these more strict thresholds we aimed to ensure that the selected bins were extremely divergent between
990 castle-building and non-castle-building species. Additionally, a higher threshold was selected for the rock-castle
991 than the pit-castle comparison because of the greater evolutionary distance and thus greater overall F_{ST} .
992 Finally, genes that were within 25kb of these bins meeting these thresholds were identified using bcftools v1.11
993 with the closest command and the *M. zebra* genome as reference. Genes within 25kb of highly divergent pit-
994 castle and rock-castle bins are referred to here as “castle-divergent”.

995 *CDG co-expression and module analysis*

996 Modules of co-expressed CDGs were analyzed using weighted correlation network analysis (WGCNA) using
997 the “WGCNA” v1.70-3 package in R. CDGs that were not observed in any nucleus were excluded from analysis.
998 The normalized gene expression data for CDGs was used as the input gene expression matrix and the function
999 pickSoftThreshold was used to determine the optimal soft-thresholding power. We determined the optimal soft-
1000 thresholding power to be 1 because it was the lowest power for which the scale-free topology fit index reached
1001 0.90. Then an adjacency matrix was created from the input gene expression matrix using the adjacency function
1002 with power = 1, type = “signed” and otherwise default parameters. The adjacency matrix was used as the
1003 topological overlap matrix (TOM) and the dissimilarity matrix was calculated as $1 - \text{TOM}$. To detect modules,
1004 k-means clustering was performed using all possible values of k and the results were compared to determine
1005 the optimal k. First, a distance matrix was constructed from the dissimilarity matrix produced by WGCNA using
1006 the dist function in R. Next, the function pam from the R package “cluster” v2.1.0 was used to cluster the
1007 distance matrix with diss = T, otherwise default parameters, and k set to the value that produced the highest
1008 average silhouette width for all genes. Briefly, silhouette width is a measure of the similarity of the genes within
1009 a module to the genes outside the module, and higher values indicate better clustering. We found that k=2,
1010 had the greatest average silhouette width. The strength of the module was evaluated using a two-sampled
1011 Welch t-test comparing the silhouette width and gene-gene correlations for CDGs within the module versus
1012 CDGs outside the module. To analyze the relationship between the CDG module and signatures of RG
1013 quiescence, the correlation coefficient was calculated based the number of genes in the CDG module
1014 expressed in each nucleus versus the number of quiescent markers expressed in each nucleus. We compared
1015 the correlation coefficient against a permuted null distribution by randomly shuffling the expression values of
1016 each gene in the module 10,000 times.

1017 *Spatial transcriptomic pre-processing and quality control*

1018 Base Call files were demultiplexed into FASTQ files and processed with Space Ranger v1.3.1 (10X Genomics).
1019 Reads were aligned to the *M. zebra* umd2a reference assembly as described above for snRNA-seq (Conte et
1020 al. 2019). Following these steps, Space Ranger generated three filtered feature-barcode matrices containing
1021 expression data for a total of 32,471 features (corresponding to annotated genes). Spots with 0 UMIs were
1022 removed resulting in 6,707 spots used in downstream analysis.

1023 *Spatial integration of snRNA-seq clusters*

1024 To predict locations of specific snRNA-seq identified clusters in spatial transcriptomics data, an ‘anchor’-based
1025 integration workflow in Seurat was used. First, both the snRNA-seq and spatial data were normalized using the
1026 SCTransform in Seurat. Next, anchors were identified between the reference snRNA-seq and the query spatial
1027 data using FindTransferAnchors in Seurat, and a matrix of predictions scores was generated for each cluster
1028 in every spot using the TransferData function in Seurat. The maximum prediction score across clusters was
1029 not uniform, therefore we normalized the values between 0 and 1 in order to enable meaningful comparisons
1030 across cell types.

1032 *Cell-cell communication analysis*

1033
1034 To assess the connectivity of cell populations, cell-cell communication analysis was performed using the R
1035 package CellChat v1.5.0. Briefly, CellChat estimates the strength of potential connection between
1036 populations from a gene expression matrix based on a database of human ligand-receptor interactions. In
1037 order to find the connection strengths between primary and secondary clusters, the gene expression matrix
1038 was duplicated and the cells in the first copy were assigned the primary labels and the cells in the second
1039 copy were assigned secondary labels. We also sought to analyze connections among additional gene-
1040 defined populations that demonstrated behavior-associated IEG expression. To achieve this, the gene
1041 expression matrices for cells from these populations were duplicated again. Therefore, before connection
1042 strengths were evaluated, the human orthologs of the *M. zebra* gene names in the gene expression matrix
1043 were found. Since, the gene expression matrix does not allow for duplicate gene names, e.g. many-to-one
1044 orthologs, values for the many-to-one ortholog with the greatest number of normalized counts were kept and
1045 others were excluded from analysis. Next, a CellChat object was created using the createCellChat function.

1046 Over-expressed genes and over-expressed interactions were found using the `identifyOverExpressedGenes`
1047 and `identifyOverExpressedInteractions` functions respectively. Next, connection strengths were calculated
1048 using the `computeCommunProb` function with the method for computing the average gene expression per
1049 cell group set to `truncatedMean`, trim set to 0.1, and `population.size` set to `FALSE`. Then, the cellular
1050 communication network was inferred and aggregated using the `filterCommunication` and `aggregateNet`
1051 functions. The receptor-ligand and the signalling pathway weights were saved using `subsetCommunication`
1052 with the `slot.name` parameter set to 'net' and `netP` respectively.

1053

1054 *Regularized Multiple Mediation Analysis*

1055

1056 Regularized multiple mediation analysis was performed using the R package `mma` v10.6-1 (Q. Yu and Li 2017).
1057 Briefly, this analysis used a regularization approach to test if one or more mediators explained the relationship
1058 between building and 8.4_Glut:8.1_Glut neuronal rebalancing, and between building and RG_2 *wdr73*
1059 expression. The following variables were considered as possible mediators of building-associated
1060 8.4_Glut:8.1_Glut neuronal rebalancing: GSI, quivering, RG_1 *wdr73* expression, RG_2 *wdr73* expression, RG_2
1061 CDG module score, RG_8 CDG module score, RG_3 *cyp19a1* expression, RG_4 proportion, IEG score in all ten
1062 build-IEG+ populations, and IEG score in 8.1_Glut and 8.4_Glut. To investigate possible mediators of RG_2
1063 *wdr73* expression, the same variables were analyzed, except RG_2 *wdr73* expression and RG_2 CDG module
1064 (which contains *wdr73*) score were excluded as possible mediators. The analysis was performed with `testtype`
1065 = 1 (LASSO) and `alpha1` and `alpha2` both set to 0.05.

1066 **REFERENCES**

- 1067 Adkins-Regan, Elizabeth. 2013. *Hormones and Animal Social Behavior*. Princeton University Press.
- 1068 Adolf, Birgit, Prisca Chapouton, Chen Sok Lam, Stefanie Topp, Birgit Tannhäuser, Uwe Strähle, Magdalena
1069 Götz, and Laure Bally-Cuif. 2006. "Conserved and Acquired Features of Adult Neurogenesis in the Zebrafish
1070 Telencephalon." *Developmental Biology* 295 (1): 278–93.
- 1071 Almlı, Lynn M., and Walter Wilczynski. 2012. "Socially Modulated Cell Proliferation Is Independent of Gonadal
1072 Steroid Hormones in the Brain of the Adult Green Treefrog (*Hyla Cinerea*)." *Brain, Behavior and Evolution* 79
1073 (3): 170–80.
- 1074 Alward, Beau A., Austin T. Hilliard, Ryan A. York, and Russell D. Fernald. 2019. "Hormonal Regulation of Social
1075 Ascent and Temporal Patterns of Behavior in an African Cichlid." *Hormones and Behavior* 107 (January): 83–
1076 95.
- 1077 Amadei, Elizabeth A., Zachary V. Johnson, Yong Jun Kwon, Aaron C. Shpiner, Varun Saravanan, Wittney D.
1078 Mays, Steven J. Ryan, et al. 2017. "Dynamic Corticostriatal Activity Biases Social Bonding in Monogamous
1079 Female Prairie Voles." *Nature* 546 (7657): 297–301.
- 1080 Amenyogbe, Eric, Gang Chen, Zhongliang Wang, Xiaoying Lu, Mingde Lin, and Ai Ying Lin. 2020. "A Review
1081 on Sex Steroid Hormone Estrogen Receptors in Mammals and Fish." *International Journal of Endocrinology*
1082 2020 (February): 5386193.
- 1083 Anderson, David J. 2016. "Circuit Modules Linking Internal States and Social Behaviour in Flies and Mice."
1084 *Nature Reviews. Neuroscience* 17 (11): 692–704.
- 1085 Asrican, Brent, Josh Wooten, Ya-Dong Li, Luis Quintanilla, Feiran Zhang, Connor Wander, Hechen Bao, et al.
1086 2020. "Neuropeptides Modulate Local Astrocytes to Regulate Adult Hippocampal Neural Stem Cells." *Neuron*
1087 108 (2): 349-366.e6.
- 1088 Bachevalier, Jocelyne, and Katherine A. Loveland. 2006. "The Orbitofrontal-Amygdala Circuit and Self-
1089 Regulation of Social-Emotional Behavior in Autism." *Neuroscience and Biobehavioral Reviews* 30 (1): 97–117.
- 1090 Badurek, Sylvia, Marilena Griguoli, Aman Asif-Malik, Barbara Zonta, Fei Guo, Silvia Middei, Laura Lagostena,
1091 et al. 2020. "Immature Dentate Granule Cells Require Ntrk2/TrkB for the Formation of Functional Hippocampal
1092 Circuitry." *iScience* 23 (5): 101078.
- 1093 Balthazart, Jacques, and Gregory F. Ball. 2016. "Endocrine and Social Regulation of Adult Neurogenesis in
1094 Songbirds." *Frontiers in Neuroendocrinology* 41 (April): 3–22.
- 1095 Baran, Nicole M., and J. Todd Strelman. 2020. "Ecotype Differences in Aggression, Neural Activity and
1096 Behaviorally Relevant Gene Expression in Cichlid Fish." *Genes, Brain, and Behavior* 19 (6): e12657.
- 1097 Barha, Cindy K., and Liisa A. M. Galea. 2010. "Influence of Different Estrogens on Neuroplasticity and Cognition
1098 in the Hippocampus." *Biochimica et Biophysica Acta* 1800 (10): 1056–67.
- 1099 Bedos, M., W. Portillo, and R. G. Paredes. 2018. "Neurogenesis and Sexual Behavior." *Frontiers in*
1100 *Neuroendocrinology* 51 (October): 68–79.
- 1101 Bendesky, Andres, Young-Mi Kwon, Jean-Marc Lassance, Caitlin L. Lewarch, Shenqin Yao, Brant K. Peterson,
1102 Meng Xiao He, Catherine Dulac, and Hopi E. Hoekstra. 2017. "The Genetic Basis of Parental Care Evolution
1103 in Monogamous Mice." *Nature* 544 (7651): 434–39.
- 1104 Berg, P. R., B. Star, C. Pampoulie, I. R. Bradbury, P. Bentzen, J. A. Hutchings, S. Jentoft, and K. S. Jakobsen.
1105 2017. "Trans-Oceanic Genomic Divergence of Atlantic Cod Ecotypes Is Associated with Large Inversions."
1106 *Heredity* 119 (6): 418–28.

- 1107 Bingman, Verner P., Cosme Salas, and Fernando Rodriguez. 2008. "Evolution of the Hippocampus." In
1108 *Encyclopedia of Neuroscience*, 1356–60. Berlin, Heidelberg: Springer Berlin Heidelberg.
- 1109 Boender, Arjen J., and Larry J. Young. 2020. "Oxytocin, Vasopressin and Social Behavior in the Age of Genome
1110 Editing: A Comparative Perspective." *Hormones and Behavior* 124 (104780): 104780.
- 1111 Brenowitz, Eliot A., and Tracy A. Larson. 2015. "Neurogenesis in the Adult Avian Song-Control System." *Cold
1112 Spring Harbor Perspectives in Biology* 7 (6): a019000.
- 1113 Brenowitz, Eliot A., and Harold H. Zakon. 2015. "Emerging from the Bottleneck: Benefits of the Comparative
1114 Approach to Modern Neuroscience." *Trends in Neurosciences* 38 (5): 273–78.
- 1115 Brinton, Roberta Diaz. 2009. "Estrogen-Induced Plasticity from Cells to Circuits: Predictions for Cognitive
1116 Function." *Trends in Pharmacological Sciences* 30 (4): 212–22.
- 1117 Chen, Xi, Xiao Li, Yin Ting Wong, Xuejiao Zheng, Haitao Wang, Yujie Peng, Hemin Feng, et al. 2019.
1118 "Cholecystokinin Release Triggered by NMDA Receptors Produces LTP and Sound-Sound Associative
1119 Memory." *Proceedings of the National Academy of Sciences of the United States of America* 116 (13): 6397–
1120 6406.
- 1121 Clark, P. J., W. J. Brzezinska, M. W. Thomas, N. A. Ryzhenko, S. A. Toshkov, and J. S. Rhodes. 2008. "Intact
1122 Neurogenesis Is Required for Benefits of Exercise on Spatial Memory but Not Motor Performance or Contextual
1123 Fear Conditioning in C57BL/6J Mice." *Neuroscience* 155 (4): 1048–58.
- 1124 Clelland, C. D., M. Choi, C. Romberg, G. D. Clemenson Jr, A. Fragniere, P. Tyers, S. Jessberger, et al. 2009.
1125 "A Functional Role for Adult Hippocampal Neurogenesis in Spatial Pattern Separation." *Science (New York,
1126 N.Y.)* 325 (5937): 210–13.
- 1127 Conte, Matthew A., Rajesh Joshi, Emily C. Moore, Sri Pratima Nandamuri, William J. Gammerding, Reade
1128 B. Roberts, Karen L. Carleton, Sigbjørn Lien, and Thomas D. Kocher. 2019. "Chromosome-Scale Assemblies
1129 Reveal the Structural Evolution of African Cichlid Genomes." *GigaScience* 8 (4).
1130 <https://doi.org/10.1093/gigascience/giz030>.
- 1131 Corbett-Detig, Russell B., and Daniel L. Hartl. 2012. "Population Genomics of Inversion Polymorphisms in
1132 *Drosophila Melanogaster*." *PLoS Genetics* 8 (12): e1003056.
- 1133 Dias, Caroline M., and Christopher A. Walsh. 2020. "Recent Advances in Understanding the Genetic
1134 Architecture of Autism." *Annual Review of Genomics and Human Genetics* 21 (1): 289–304.
- 1135 Dimitrov, Daniel, Dénes Túrei, Martin Garrido-Rodriguez, Paul L. Burmedi, James S. Nagai, Charlotte Boys,
1136 Ricardo O. Ramirez Flores, et al. 2022. "Comparison of Methods and Resources for Cell-Cell Communication
1137 Inference from Single-Cell RNA-Seq Data." *Nature Communications* 13 (1): 3224.
- 1138 Diotel, Nicolas, Colette Vaillant, Cyril Gabbero, Svetlana Mironov, Alexis Fostier, Marie-Madeleine Gueguen,
1139 Isabelle Anglade, Olivier Kah, and Elisabeth Pellegrini. 2013. "Effects of Estradiol in Adult Neurogenesis and
1140 Brain Repair in Zebrafish." *Hormones and Behavior* 63 (2): 193–207.
- 1141 Duarte-Guterman, Paula, Shunya Yagi, Carmen Chow, and Liisa A. M. Galea. 2015. "Hippocampal Learning,
1142 Memory, and Neurogenesis: Effects of Sex and Estrogens across the Lifespan in Adults." *Hormones and
1143 Behavior* 74 (August): 37–52.
- 1144 Dulac, Catherine, Lauren A. O'Connell, and Zheng Wu. 2014. "Neural Control of Maternal and Paternal
1145 Behaviors." *Science (New York, N.Y.)* 345 (6198): 765–70.
- 1146 Dunlap, Kent D., Michael Chung, and James F. Castellano. 2013. "Influence of Long-Term Social Interaction
1147 on Chirping Behavior, Steroid Levels and Neurogenesis in Weakly Electric Fish." *The Journal of Experimental
1148 Biology* 216 (Pt 13): 2434–41.

- 1149 Elliott, S. Benjamin, Erik Harvey-Girard, Ana C. C. Giassi, and Leonard Maler. 2017. "Hippocampal-like Circuitry
1150 in the Pallium of an Electric Fish: Possible Substrates for Recursive Pattern Separation and Completion." *The*
1151 *Journal of Comparative Neurology* 525 (1): 8–46.
- 1152 Engelmann, Jacob, Avner Wallach, and Leonard Maler. 2021. "Linking Active Sensing and Spatial Learning in
1153 Weakly Electric Fish." *Current Opinion in Neurobiology* 71 (December): 1–10.
- 1154 Ervin, Kelsy S. J., Jennifer M. Lymer, Richard Matta, Amy E. Clipperton-Allen, Martin Kavaliers, and Elena
1155 Choleris. 2015. "Estrogen Involvement in Social Behavior in Rodents: Rapid and Long-Term Actions."
1156 *Hormones and Behavior* 74 (August): 53–76.
- 1157 Fotowat, Haleh, Candice Lee, James Jaeyoon Jun, and Len Maler. 2019. "Neural Activity in a Hippocampus-
1158 like Region of the Teleost Pallium Is Associated with Active Sensing and Navigation." *ELife* 8 (April): e44119.
- 1159 Furth, W. R. van, G. Wolterink, and J. M. van Ree. 1995. "Regulation of Masculine Sexual Behavior:
1160 Involvement of Brain Opioids and Dopamine." *Brain Research. Brain Research Reviews* 21 (2): 162–84.
- 1161 Gallant, Jason R., and Lauren A. O'Connell. 2020. "Studying Convergent Evolution to Relate Genotype to
1162 Behavioral Phenotype." *The Journal of Experimental Biology* 223 (Pt Suppl 1): jeb213447.
- 1163 Gangopadhyay, Prabaha, Megha Chawla, Olga Dal Monte, and Steve W. C. Chang. 2021. "Prefrontal-
1164 Amygdala Circuits in Social Decision-Making." *Nature Neuroscience* 24 (1): 5–18.
- 1165 Ganz, Julia, and Michael Brand. 2016. "Adult Neurogenesis in Fish." *Cold Spring Harbor Perspectives in*
1166 *Biology* 8 (7). <https://doi.org/10.1101/cshperspect.a019018>.
- 1167 Ganz, Julia, Volker Kroehne, Dorian Freudenreich, Anja Machate, Michaela Geffarth, Ingo Braasch, Jan Kaslin,
1168 and Michael Brand. 2014. "Subdivisions of the Adult Zebrafish Pallium Based on Molecular Marker Analysis."
1169 *F1000Research* 3 (December): 308.
- 1170 Ghashghaei, H. T., Janet Weber, Larysa Pevny, Ralf Schmid, Markus H. Schwab, K. C. Kent Lloyd, David D.
1171 Eisenstat, Cary Lai, and E. S. Anton. 2006. "The Role of Neuregulin-ErbB4 Interactions on the Proliferation and
1172 Organization of Cells in the Subventricular Zone." *Proceedings of the National Academy of Sciences of the*
1173 *United States of America* 103 (6): 1930–35.
- 1174 Giassi, Ana C. C., William Ellis, and Leonard Maler. 2012. "Organization of the Gymnotiform Fish Pallium in
1175 Relation to Learning and Memory: III. Intrinsic Connections." *The Journal of Comparative Neurology* 520 (15):
1176 3369–94.
- 1177 Goldman, S. A., and F. Nottebohm. 1983. "Neuronal Production, Migration, and Differentiation in a Vocal
1178 Control Nucleus of the Adult Female Canary Brain." *Proceedings of the National Academy of Sciences of the*
1179 *United States of America* 80 (8): 2390–94.
- 1180 Goodson, James L. 2005. "The Vertebrate Social Behavior Network: Evolutionary Themes and Variations."
1181 *Hormones and Behavior* 48 (1): 11–22.
- 1182 Götz, Magdalena, and Wieland B. Huttner. 2005. "The Cell Biology of Neurogenesis." *Nature Reviews.*
1183 *Molecular Cell Biology* 6 (10): 777–88.
- 1184 Gutzeit, Vanessa A., Kyla Ahuna, Tabia L. Santos, Ashley M. Cunningham, Meghin Sadsad Rooney, Andrea
1185 Muñoz Zamora, Christine A. Denny, and Zoe R. Donaldson. 2020. "Optogenetic Reactivation of Prefrontal
1186 Social Neural Ensembles Mimics Social Buffering of Fear." *Neuropsychopharmacology: Official Publication of*
1187 *the American College of Neuropsychopharmacology* 45 (6): 1068–77.
- 1188 Guzowski, John F., Jerilyn A. Timlin, Badri Roysam, Bruce L. McNaughton, Paul F. Worley, and Carol A.
1189 Barnes. 2005. "Mapping Behaviorally Relevant Neural Circuits with Immediate-Early Gene Expression."
1190 *Current Opinion in Neurobiology* 15 (5): 599–606.

- 1191 Hasenpusch-Theil, Kerstin, Stephen West, Alexandra Kelman, Zrinko Kozic, Sophie Horrocks, Andrew P.
1192 McMahon, David J. Price, John O. Mason, and Thomas Theil. 2018. "Gli3 Controls the Onset of Cortical
1193 Neurogenesis by Regulating the Radial Glial Cell Cycle through Cdk6 Expression." *Development (Cambridge,
1194 England)* 145 (17): dev163147.
- 1195 Heinrichs, Markus, and Jens Gaab. 2007. "Neuroendocrine Mechanisms of Stress and Social Interaction:
1196 Implications for Mental Disorders." *Current Opinion in Psychiatry* 20 (2): 158–62.
- 1197 Hoffmann, Ary A., and Loren H. Rieseberg. 2008. "Revisiting the Impact of Inversions in Evolution: From
1198 Population Genetic Markers to Drivers of Adaptive Shifts and Speciation?" *Annual Review of Ecology,
1199 Evolution, and Systematics* 39 (1): 21–42.
- 1200 Hofmann, Hans A., Annaliese K. Beery, Daniel T. Blumstein, Iain D. Couzin, Ryan L. Earley, Loren D. Hayes,
1201 Peter L. Hurd, et al. 2014. "An Evolutionary Framework for Studying Mechanisms of Social Behavior." *Trends
1202 in Ecology & Evolution* 29 (10): 581–89.
- 1203 Howe, Kerstin, Matthew D. Clark, Carlos F. Torroja, James Torrance, Camille Berthelot, Matthieu Muffato, John
1204 E. Collins, et al. 2013. "The Zebrafish Reference Genome Sequence and Its Relationship to the Human
1205 Genome." *Nature* 496 (7446): 498–503.
- 1206 Huang, Kaichi, and Loren H. Rieseberg. 2020. "Frequency, Origins, and Evolutionary Role of Chromosomal
1207 Inversions in Plants." *Frontiers in Plant Science* 11 (March): 296.
- 1208 Huffman, Lin S., Lauren A. O'Connell, and Hans A. Hofmann. 2013. "Aromatase Regulates Aggression in the
1209 African Cichlid Fish *Astatotilapia Burtoni*." *Physiology & Behavior* 112–113 (March): 77–83.
- 1210 Hung, Lin W., Sophie Neuner, Jai S. Polepalli, Kevin T. Beier, Matthew Wright, Jessica J. Walsh, Eastman M.
1211 Lewis, et al. 2017. "Gating of Social Reward by Oxytocin in the Ventral Tegmental Area." *Science (New York,
1212 N.Y.)* 357 (6358): 1406–11.
- 1213 Ikeda, Kazuhiro, Kuniko Horie-Inoue, and Satoshi Inoue. 2015. "Identification of Estrogen-Responsive Genes
1214 Based on the DNA Binding Properties of Estrogen Receptors Using High-Throughput Sequencing Technology." *Acta Pharmacologica Sinica* 36 (1): 24–31.
- 1216 Ishii, Kentaro K., and Kazushige Touhara. 2019. "Neural Circuits Regulating Sexual Behaviors via the Olfactory
1217 System in Mice." *Neuroscience Research* 140 (March): 59–76.
- 1218 Jerber, Julie, Daniel D. Seaton, Anna S. E. Cuomo, Natsuhiko Kumasaka, James Haldane, Juliette Steer, Minal
1219 Patel, et al. 2021. "Population-Scale Single-Cell RNA-Seq Profiling across Dopaminergic Neuron
1220 Differentiation." *Nature Genetics* 53 (3): 304–12.
- 1221 Jin, Suoqin, Christian F. Guerrero-Juarez, Lihua Zhang, Ivan Chang, Raul Ramos, Chen-Hsiang Kuan, Peggy
1222 Myung, Maksim V. Plikus, and Qing Nie. 2021. "Inference and Analysis of Cell-Cell Communication Using
1223 CellChat." *Nature Communications* 12 (1): 1088.
- 1224 Johnson, Zachary V., Manu Tej Sharma Arrojwala, Vineeth Aljapur, Tyrone Lee, Tucker J. Lancaster, Mark C.
1225 Lowder, Karen Gu, et al. 2020. "Automated Measurement of Long-Term Bower Behaviors in Lake Malawi
1226 Cichlids Using Depth Sensing and Action Recognition." *Scientific Reports* 10 (1): 20573.
- 1227 Johnson, Zachary V., Emily C. Moore, Ryan Y. Wong, John R. Godwin, Jeffrey T. Streebman, and Reade B.
1228 Roberts. 2020. "Exploratory Behaviour Is Associated with Microhabitat and Evolutionary Radiation in Lake
1229 Malawi Cichlids." *Animal Behaviour* 160 (February): 121–34.
- 1230 Johnson, Zachary V., and Larry J. Young. 2015. "Neurobiological Mechanisms of Social Attachment and Pair
1231 Bonding." *Current Opinion in Behavioral Sciences* 3 (June): 38–44.
- 1232 ———. 2017. "Oxytocin and Vasopressin Neural Networks: Implications for Social Behavioral Diversity and
1233 Translational Neuroscience." *Neuroscience and Biobehavioral Reviews* 76 (Pt A): 87–98.

- 1234 ———. 2018. “Evolutionary Diversity as a Catalyst for Biological Discovery.” *Integrative Zoology* 13 (6): 616–
1235 33.
- 1236 Jourjine, Nicholas, and Hopi E. Hoekstra. 2021. “Expanding Evolutionary Neuroscience: Insights from
1237 Comparing Variation in Behavior.” *Neuron* 109 (7): 1084–99.
- 1238 Juntti, Scott. 2019. “The Future of Gene-Guided Neuroscience Research in Non-Traditional Model Organisms.”
1239 *Brain, Behavior and Evolution* 93 (2–3): 108–21.
- 1240 Juntti, Scott A., Austin T. Hilliard, Kai R. Kent, Anusha Kumar, Andrew Nguyen, Mariana A. Jimenez, Jasmine
1241 L. Loveland, Philippe Mourrain, and Russell D. Fernald. 2016. “A Neural Basis for Control of Cichlid Female
1242 Reproductive Behavior by Prostaglandin F_{2α}.” *Current Biology: CB* 26 (7): 943–49.
- 1243 Jurisch-Yaksi, Nathalie, Emre Yaksi, and Caghan Kizil. 2020. “Radial Glia in the Zebrafish Brain: Functional,
1244 Structural, and Physiological Comparison with the Mammalian Glia.” *Glia* 68 (12): 2451–70.
- 1245 Káradóttir, Ragnhildur T., and Chay T. Kuo. 2018. “Neuronal Activity-Dependent Control of Postnatal
1246 Neurogenesis and Gliogenesis.” *Annual Review of Neuroscience* 41 (July): 139–61.
- 1247 Kastanenka, Ksenia V., Rubén Moreno-Bote, Maurizio De Pittà, Gertrudis Perea, Abel Eraso-Pichot, Roser
1248 Masgrau, Kira E. Poskanzer, and Elena Galea. 2020. “A Roadmap to Integrate Astrocytes into Systems
1249 Neuroscience.” *Glia* 68 (1): 5–26.
- 1250 Keifer, Joyce, and Cliff H. Summers. 2016. “Putting the ‘Biology’ Back into ‘Neurobiology’: The Strength of
1251 Diversity in Animal Model Systems for Neuroscience Research.” *Frontiers in Systems Neuroscience* 10
1252 (August): 69.
- 1253 Keleman, Krystyna, Eleftheria Vrontou, Sebastian Krüttner, Jai Y. Yu, Amina Kurtovic-Kozaric, and Barry J.
1254 Dickson. 2012. “Dopamine Neurons Modulate Pheromone Responses in Drosophila Courtship Learning.”
1255 *Nature* 489 (7414): 145–49.
- 1256 Kelly, Martin J., and Oline K. Rønnekleiv. 2009. “Control of CNS Neuronal Excitability by Estrogens via
1257 Membrane-Initiated Signaling.” *Molecular and Cellular Endocrinology* 308 (1–2): 17–25.
- 1258 Kennedy, Daniel P., and Ralph Adolphs. 2012. “The Social Brain in Psychiatric and Neurological Disorders.”
1259 *Trends in Cognitive Sciences* 16 (11): 559–72.
- 1260 Kimchi, Tali, Jennings Xu, and Catherine Dulac. 2007. “A Functional Circuit Underlying Male Sexual Behaviour
1261 in the Female Mouse Brain.” *Nature* 448 (7157): 1009–14.
- 1262 Kirchshofer, Rosa. 1953. “Aktionssystem Des Maulbrütters Haplochromis Desfontainesii.” *Zeitschrift Für
1263 Tierpsychologie* 10 (2): 297–318.
- 1264 Kirkpatrick, Mark, and Nick Barton. 2006. “Chromosome Inversions, Local Adaptation and Speciation.”
1265 *Genetics* 173 (1): 419–34.
- 1266 Klinge, C. M. 2001. “Estrogen Receptor Interaction with Estrogen Response Elements.” *Nucleic Acids
1267 Research* 29 (14): 2905–19.
- 1268 Kohl, Johannes, Benedicte M. Babayan, Nimrod D. Rubinstein, Anita E. Autry, Brenda Marin-Rodriguez,
1269 Vikrant Kapoor, Kazunari Miyamishi, et al. 2018. “Functional Circuit Architecture Underlying Parental
1270 Behaviour.” *Nature* 556 (7701): 326–31.
- 1271 Küpper, Clemens, Michael Stocks, Judith E. Risse, Natalie Dos Remedios, Lindsay L. Farrell, Susan B. McRae,
1272 Tawna C. Morgan, et al. 2016. “A Supergene Determines Highly Divergent Male Reproductive Morphs in the
1273 Ruff.” *Nature Genetics* 48 (1): 79–83.
- 1274 Labusch, Miriam, Laure Mancini, David Morizet, and Laure Bally-Cuif. 2020. “Conserved and Divergent
1275 Features of Adult Neurogenesis in Zebrafish.” *Frontiers in Cell and Developmental Biology* 8 (June): 525.

- 1276 Lacar, Benjamin, Sara B. Linker, Baptiste N. Jaeger, Suguna Krishnaswami, Jerika Barron, Martijn Kelder,
1277 Sarah Parylak, et al. 2016. "Nuclear RNA-Seq of Single Neurons Reveals Molecular Signatures of Activation."
1278 *Nature Communications* 7 (April): 11022.
- 1279 Lamichhaney, Sangeet, Guangyi Fan, Fredrik Widemo, Ulrika Gunnarsson, Doreen Schwochow Thalmann,
1280 Marc P. Hoepfner, Susanne Kerje, et al. 2016. "Structural Genomic Changes Underlie Alternative
1281 Reproductive Strategies in the Ruff (*Philomachus Pugnax*)." *Nature Genetics* 48 (1): 84–88.
- 1282 Langfelder, Peter, and Steve Horvath. 2008. "WGCNA: An R Package for Weighted Correlation Network
1283 Analysis." *BMC Bioinformatics* 9 (1): 559.
- 1284 Laurent, Gilles. 2020. "On the Value of Model Diversity in Neuroscience." *Nature Reviews. Neuroscience* 21
1285 (8): 395–96.
- 1286 Lévy, Frederic, Martine Batailler, Maryse Meurisse, and Martine Migaud. 2017. "Adult Neurogenesis in Sheep:
1287 Characterization and Contribution to Reproduction and Behavior." *Frontiers in Neuroscience* 11 (October): 570.
- 1288 Lipsky, Robert H., and Ann M. Marini. 2007. "Brain-Derived Neurotrophic Factor in Neuronal Survival and
1289 Behavior-Related Plasticity." *Annals of the New York Academy of Sciences* 1122 (1): 130–43.
- 1290 Loh, Yong-Hwee E., Lee S. Katz, Meryl C. Mims, Thomas D. Kocher, Soojin V. Yi, and J. Todd Strelman.
1291 2008. "Comparative Analysis Reveals Signatures of Differentiation amid Genomic Polymorphism in Lake
1292 Malawi Cichlids." *Genome Biology* 9 (7): R113.
- 1293 Long, Lijiang, Zachary V. Johnson, Junyu Li, Tucker J. Lancaster, Vineeth Aljapur, Jeffrey T. Strelman, and
1294 Patrick T. McGrath. 2020. "Automatic Classification of Cichlid Behaviors Using 3D Convolutional Residual
1295 Networks." *IScience* 23 (10): 101591.
- 1296 Louhivuori, Lauri M., Pauli M. Turunen, Verna Louhivuori, Venkatram Yellapragada, Tommy Nordström, Per
1297 Uhlén, and Karl E. Åkerman. 2018. "Regulation of Radial Glial Process Growth by Glutamate via
1298 MGlur5/TRPC3 and Neuregulin/ErbB4." *Glia* 66 (1): 94–107.
- 1299 Louilot, A., J. L. Gonzalez-Mora, T. Guadalupe, and M. Mas. 1991. "Sex-Related Olfactory Stimuli Induce a
1300 Selective Increase in Dopamine Release in the Nucleus Accumbens of Male Rats. A Voltammetric Study."
1301 *Brain Research* 553 (2): 313–17.
- 1302 Lukaszewicz, Agnès I., and David J. Anderson. 2011. "Cyclin D1 Promotes Neurogenesis in the Developing
1303 Spinal Cord in a Cell Cycle-Independent Manner." *Proceedings of the National Academy of Sciences of the
1304 United States of America* 108 (28): 11632–37.
- 1305 Lyons, Michelle R., and Anne E. West. 2011. "Mechanisms of Specificity in Neuronal Activity-Regulated Gene
1306 Transcription." *Progress in Neurobiology* 94 (3): 259–95.
- 1307 Malinsky, Milan, Hannes Svoldal, Alexandra M. Tyers, Eric A. Miska, Martin J. Genner, George F. Turner, and
1308 Richard Durbin. 2018. "Whole-Genome Sequences of Malawi Cichlids Reveal Multiple Radiations
1309 Interconnected by Gene Flow." *Nature Ecology & Evolution* 2 (12): 1940–55.
- 1310 Maney, Donna L., Jennifer R. Merritt, Mackenzie R. Prichard, Brent M. Horton, and Soojin V. Yi. 2020. "Inside
1311 the Supergene of the Bird with Four Sexes." *Hormones and Behavior* 126 (104850): 104850.
- 1312 Martelotto, Luciano G. 2020. "'Frankenstein' Protocol for Nuclei Isolation from Fresh and Frozen Tissue for
1313 SnRNAseq Protocol Guidelines." Protocols.io. December 21, 2020. <https://www.protocols.io/view/frankensteins-protocol-for-nuclei-isolation-from-f-5jyl8nx98l2w/v3/guidelines>.
- 1314
- 1315 Martinelli, David C., Kylie S. Chew, Astrid Rohlmann, Matthew Y. Lum, Susanne Ressler, Samer Hattar, Axel T.
1316 Brunger, Markus Missler, and Thomas C. Südhof. 2016. "Expression of C1ql3 in Discrete Neuronal Populations
1317 Controls Efferent Synapse Numbers and Diverse Behaviors." *Neuron* 91 (5): 1034–51.

- 1318 Maruska, Karen P., Julie M. Butler, Karen E. Field, and Danielle T. Porter. 2017. "Localization of Glutamatergic,
1319 GABAergic, and Cholinergic Neurons in the Brain of the African Cichlid Fish, *Astatotilapia Burtoni*." *The Journal*
1320 *of Comparative Neurology* 525 (3): 610–38.
- 1321 Maruska, Karen P., Russ E. Carpenter, and Russell D. Fernald. 2012. "Characterization of Cell Proliferation
1322 throughout the Brain of the African Cichlid Fish *Astatotilapia Burtoni* and Its Regulation by Social Status." *The*
1323 *Journal of Comparative Neurology* 520 (15): 3471–91.
- 1324 Maruska, Karen P., and Russell D. Fernald. 2010. "Behavioral and Physiological Plasticity: Rapid Changes
1325 during Social Ascent in an African Cichlid Fish." *Hormones and Behavior* 58 (2): 230–40.
- 1326 McKaye, Kenneth R., Svata M. Louda, and Jay R. Stauffer Jr. 1990. "Bower Size and Male Reproductive
1327 Success in a Cichlid Fish Lek." *The American Naturalist* 135 (5): 597–613.
- 1328 Merritt, Jennifer R., Kathleen E. Grogan, Wendy M. Zinzow-Kramer, Dan Sun, Eric A. Ortlund, Soojin V. Yi,
1329 and Donna L. Maney. 2020. "A Supergene-Linked Estrogen Receptor Drives Alternative Phenotypes in a
1330 Polymorphic Songbird." *Proceedings of the National Academy of Sciences of the United States of America* 117
1331 (35): 21673–80.
- 1332 Miller, Jonathan, Andrew J. Watrous, Melina Tsitsiklis, Sang Ah Lee, Sameer A. Sheth, Catherine A. Schevon,
1333 Elliot H. Smith, et al. 2018. "Lateralized Hippocampal Oscillations Underlie Distinct Aspects of Human Spatial
1334 Memory and Navigation." *Nature Communications* 9 (1): 1–12.
- 1335 Mira, Helena, and Javier Morante. 2020. "Neurogenesis from Embryo to Adult - Lessons from Flies and Mice."
1336 *Frontiers in Cell and Developmental Biology* 8 (June): 533.
- 1337 Moffitt, Jeffrey R., Dhananjay Bambah-Mukku, Stephen W. Eichhorn, Eric Vaughn, Karthik Shekhar, Julio D.
1338 Perez, Nimrod D. Rubinstein, et al. 2018. "Molecular, Spatial, and Functional Single-Cell Profiling of the
1339 Hypothalamic Preoptic Region." *Science* 362 (6416). <https://doi.org/10.1126/science.aau5324>.
- 1340 Moreira, Frederico, Tim-Rasmus Kiehl, Kelvin So, Norbert F. Ajeawung, Carmelita Honculada, Peter Gould,
1341 Russell O. Pieper, and Deepak Kamnasaran. 2011. "NPAS3 Demonstrates Features of a Tumor Suppressive
1342 Role in Driving the Progression of Astrocytomas." *The American Journal of Pathology* 179 (1): 462–76.
- 1343 Nagai, Jun, Xinzhu Yu, Thomas Papouin, Eunji Cheong, Marc R. Freeman, Kelly R. Monk, Michael H. Hastings,
1344 et al. 2021. "Behaviorally Consequential Astrocytic Regulation of Neural Circuits." *Neuron* 109 (4): 576–96.
- 1345 Nakazawa, Kazu, Thomas J. McHugh, Matthew A. Wilson, and Susumu Tonegawa. 2004. "NMDA Receptors,
1346 Place Cells and Hippocampal Spatial Memory." *Nature Reviews. Neuroscience* 5 (5): 361–72.
- 1347 Nelson, L. R., and S. E. Bulun. 2001. "Estrogen Production and Action." *Journal of the American Academy of*
1348 *Dermatology* 45 (3 Suppl): S116-24.
- 1349 Nelson, Sacha B., and Vera Valakh. 2015. "Excitatory/Inhibitory Balance and Circuit Homeostasis in Autism
1350 Spectrum Disorders." *Neuron* 87 (4): 684–98.
- 1351 Newman, S. W. 1999. "The Medial Extended Amygdala in Male Reproductive Behavior. A Node in the
1352 Mammalian Social Behavior Network." *Annals of the New York Academy of Sciences* 877 (1 ADVANCING
1353 FRO): 242–57.
- 1354 Ocaña, Francisco M., Sara Uceda, Jorge L. Arias, Cosme Salas, and Fernando Rodríguez. 2017. "Dynamics
1355 of Goldfish Subregional Hippocampal Pallium Activity throughout Spatial Memory Formation." *Brain, Behavior*
1356 *and Evolution* 90 (2): 154–70.
- 1357 O'Connell, Lauren A., and Hans A. Hofmann. 2011a. "Genes, Hormones, and Circuits: An Integrative Approach
1358 to Study the Evolution of Social Behavior." *Frontiers in Neuroendocrinology* 32 (3): 320–35.
- 1359 ———. 2011b. "The Vertebrate Mesolimbic Reward System and Social Behavior Network: A Comparative
1360 Synthesis." *The Journal of Comparative Neurology* 519 (18): 3599–3639.

- 1361 O'Connell, Lauren A., Bryan J. Matthews, and Hans A. Hofmann. 2012. "Isotocin Regulates Paternal Care in a
1362 Monogamous Cichlid Fish." *Hormones and Behavior* 61 (5): 725–33.
- 1363 Ogawa, S., A. E. Chester, S. C. Hewitt, V. R. Walker, J. A. Gustafsson, O. Smithies, K. S. Korach, and D. W.
1364 Pfaff. 2000. "Abolition of Male Sexual Behaviors in Mice Lacking Estrogen Receptors Alpha and Beta (Alpha
1365 Beta ERKO)." *Proceedings of the National Academy of Sciences of the United States of America* 97 (26):
1366 14737–41.
- 1367 Ogawa, Sonoko, Shinji Tsukahara, Elena Choleris, and Nandini Vasudevan. 2020. "Estrogenic Regulation of
1368 Social Behavior and Sexually Dimorphic Brain Formation." *Neuroscience and Biobehavioral Reviews* 110
1369 (March): 46–59.
- 1370 Pardal, Ricardo, and José López Barneo. 2016. "Mature Neurons Modulate Neurogenesis through Chemical
1371 Signals Acting on Neural Stem Cells." *Development, Growth & Differentiation* 58 (5): 456–62.
- 1372 Patil, Chinar, Jonathan B. Sylvester, Kawther Abdilleh, Michael W. Norsworthy, Karen Pottin, Milan Malinsky,
1373 Ryan F. Bloomquist, Zachary V. Johnson, Patrick T. McGrath, and Jeffrey T. Strelman. 2021. "Genome-
1374 Enabled Discovery of Evolutionary Divergence in Brains and Behavior." *Scientific Reports* 11 (1): 13016.
- 1375 Pellegrini, Elisabeth, Nicolas Diotel, Colette Vaillant-Capitaine, Rita Pérez Maria, Marie-Madeleine Gueguen,
1376 Ahmed Nasri, Joel Cano Nicolau, and Olivier Kah. 2016. "Steroid Modulation of Neurogenesis: Focus on Radial
1377 Glial Cells in Zebrafish." *The Journal of Steroid Biochemistry and Molecular Biology* 160 (June): 27–36.
- 1378 Pfenning, Andreas R., Erina Hara, Osceola Whitney, Miriam V. Rivas, Rui Wang, Petra L. Roulhac, Jason T.
1379 Howard, et al. 2014. "Convergent Transcriptional Specializations in the Brains of Humans and Song-Learning
1380 Birds." *Science (New York, N. Y.)* 346 (6215): 1256846.
- 1381 Purcell, Jessica, Alan Brelsford, Yannick Wurm, Nicolas Perrin, and Michel Chapuisat. 2014. "Convergent
1382 Genetic Architecture Underlies Social Organization in Ants." *Current Biology: CB* 24 (22): 2728–32.
- 1383 Raj, Bushra, Daniel E. Wagner, Aaron McKenna, Shristi Pandey, Allon M. Klein, Jay Shendure, James A.
1384 Gagnon, and Alexander F. Schier. 2018. "Simultaneous Single-Cell Profiling of Lineages and Cell Types in the
1385 Vertebrate Brain." *Nature Biotechnology* 36 (5): 442–50.
- 1386 Ramallo, Martín R., Agustina Birba, Renato M. Honji, Leonel Morandini, Renata G. Moreira, Gustavo M.
1387 Somoza, and Matías Pandolfi. 2015. "A Multidisciplinary Study on Social Status and the Relationship between
1388 Inter-Individual Variation in Hormone Levels and Agonistic Behavior in a Neotropical Cichlid Fish." *Hormones
1389 and Behavior* 69 (March): 139–51.
- 1390 Ribbink, A. J., B. A. Marsh, A. C. Marsh, A. C. Ribbink, and B. J. Sharp. 1983. "A Preliminary Survey of the
1391 Cichlid Fishes of Rocky Habitats in Lake Malawi." *South African Journal of Zoology* 18 (3): 149–310.
- 1392 Robinson, Gene E., Russell D. Fernald, and David F. Clayton. 2008. "Genes and Social Behavior." *Science
1393 (New York, N. Y.)* 322 (5903): 896–900.
- 1394 Rodríguez, Fernando, J. Carlos López, J. Pedro Vargas, Yolanda Gómez, Cristina Broglio, and Cosme Salas.
1395 2002. "Conservation of Spatial Memory Function in the Pallial Forebrain of Reptiles and Ray-Finned Fishes."
1396 *The Journal of Neuroscience: The Official Journal of the Society for Neuroscience* 22 (7): 2894–2903.
- 1397 Roesti, Marius, Benjamin Kueng, Dario Moser, and Daniel Berner. 2015. "The Genomics of Ecological
1398 Vicariance in Threespine Stickleback Fish." *Nature Communications* 6 (1): 8767.
- 1399 Salas, Cosme, Cristina Broglio, Emilio Durán, Francisco M. Ocaña, Isabel Martín-Monzón, Antonia Gómez,
1400 and Fernando Rodríguez. 2017. "Spatial Learning and Its Neural Basis in Fish ☆." In *Learning and Memory: A
1401 Comprehensive Reference*, 347–73. Elsevier.
- 1402 Salzburger, Walter. 2018. "Understanding Explosive Diversification through Cichlid Fish Genomics." *Nature
1403 Reviews. Genetics* 19 (11): 705–17.

- 1404 Santello, Mirko, Nicolas Toni, and Andrea Volterra. 2019. "Astrocyte Function from Information Processing to
1405 Cognition and Cognitive Impairment." *Nature Neuroscience* 22 (2): 154–66.
- 1406 Sarkar, Saumyendra N., Ren-Qi Huang, Shaun M. Logan, Kun Don Yi, Glenn H. Dillon, and James W.
1407 Simpkins. 2008. "Estrogens Directly Potentiate Neuronal L-Type Ca²⁺ Channels." *Proceedings of the National
1408 Academy of Sciences of the United States of America* 105 (39): 15148–53.
- 1409 Schaal, Sara M., Benjamin C. Haller, and Katie E. Lotterhos. 2022. "Inversion Invasions: When the Genetic
1410 Basis of Local Adaptation Is Concentrated within Inversions in the Face of Gene Flow." *Philosophical
1411 Transactions of the Royal Society of London. Series B, Biological Sciences* 377 (1856): 20210200.
- 1412 Schiller, Crystal Edler, Samantha Meltzer-Brody, and David R. Rubinow. 2015. "The Role of Reproductive
1413 Hormones in Postpartum Depression." *CNS Spectrums* 20 (1): 48–59.
- 1414 Shin, Jaehoon, Daniel A. Berg, Yunhua Zhu, Joseph Y. Shin, Juan Song, Michael A. Bonaguidi, Grigori
1415 Enikolopov, et al. 2015. "Single-Cell RNA-Seq with Waterfall Reveals Molecular Cascades Underlying Adult
1416 Neurogenesis." *Cell Stem Cell* 17 (3): 360–72.
- 1417 Silva, Vinicius H. da, Veronika N. Laine, Mirte Bosse, Lewis G. Spurgin, Martijn F. L. Derks, Kees van Oers,
1418 Bert Dibbits, et al. 2019. "The Genomic Complexity of a Large Inversion in Great Tits." *Genome Biology and
1419 Evolution* 11 (7): 1870–81.
- 1420 Smith, Caroline C., Lindsey C. Vedder, and Lori L. McMahon. 2009. "Estradiol and the Relationship between
1421 Dendritic Spines, NR2B Containing NMDA Receptors, and the Magnitude of Long-Term Potentiation at
1422 Hippocampal CA3-CA1 Synapses." *Psychoneuroendocrinology* 34 Suppl 1 (December): S130-42.
- 1423 Smith, Chris R., Amy L. Toth, Andrew V. Suarez, and Gene E. Robinson. 2008. "Genetic and Genomic
1424 Analyses of the Division of Labour in Insect Societies." *Nature Reviews. Genetics* 9 (10): 735–48.
- 1425 Soltesz, Ivan, and Attila Losonczy. 2018. "CA1 Pyramidal Cell Diversity Enabling Parallel Information
1426 Processing in the Hippocampus." *Nature Neuroscience* 21 (4): 484–93.
- 1427 Song, Juan, Reid H. J. Olsen, Jiaqi Sun, Guo-Li Ming, and Hongjun Song. 2016. "Neuronal Circuitry
1428 Mechanisms Regulating Adult Mammalian Neurogenesis." *Cold Spring Harbor Perspectives in Biology* 8 (8):
1429 a018937.
- 1430 Srivastava, Deepak P., and Peter Penzes. 2011. "Rapid Estradiol Modulation of Neuronal Connectivity and Its
1431 Implications for Disease." *Frontiers in Endocrinology* 2 (November): 77.
- 1432 Stefansson, Hreinn, Agnar Helgason, Gudmar Thorleifsson, Valgerdur Steinthorsdottir, Gisli Masson, John
1433 Barnard, Adam Baker, et al. 2005. "A Common Inversion under Selection in Europeans." *Nature Genetics* 37
1434 (2): 129–37.
- 1435 Stein, Murray B., Chia-Yen Chen, Sonia Jain, Kevin P. Jensen, Feng He, Steven G. Heeringa, Ronald C.
1436 Kessler, et al. 2017. "Genetic Risk Variants for Social Anxiety." *American Journal of Medical Genetics. Part B,
1437 Neuropsychiatric Genetics: The Official Publication of the International Society of Psychiatric Genetics* 174 (4):
1438 470–82.
- 1439 Sylvester, J. B., C. A. Rich, C. Yi, J. N. Peres, C. Houart, and J. T. Strelman. 2013. "Competing Signals Drive
1440 Telencephalon Diversity." *Nature Communications* 4: 1745.
- 1441 Tilley, F. C., C. Arrondel, C. Chhuon, M. Boisson, N. Cagnard, M. Parisot, G. Menara, et al. 2021. "Disruption
1442 of Pathways Regulated by Integrator Complex in Galloway-Mowat Syndrome Due to WDR73 Mutations."
1443 *Scientific Reports* 11 (1): 5388.
- 1444 Tosches, Maria Antonietta, Tracy M. Yamawaki, Robert K. Naumann, Ariel A. Jacobi, Georgi Tushev, and
1445 Gilles Laurent. 2018. "Evolution of Pallium, Hippocampus, and Cortical Cell Types Revealed by Single-Cell
1446 Transcriptomics in Reptiles." *Science (New York, N.Y.)* 360 (6391): 881–88.

- 1447 Tuttle, Elaina M., Alan O. Bergland, Marisa L. Korody, Michael S. Brewer, Daniel J. Newhouse, Patrick Minx,
1448 Maria Stager, et al. 2016. "Divergence and Functional Degradation of a Sex Chromosome-like Supergene."
1449 *Current Biology: CB* 26 (3): 344–50.
- 1450 Uceda, S., F. M. Ocaña, I. Martín-Monzón, B. Rodríguez-Expósito, E. Durán, and F. Rodríguez. 2015. "Spatial
1451 Learning-Related Changes in Metabolic Brain Activity Contribute to the Delimitation of the Hippocampal Pallium
1452 in Goldfish." *Behavioural Brain Research* 292 (October): 403–8.
- 1453 Vikbladh, Oliver M., Michael R. Meager, John King, Karen Blackmon, Orrin Devinsky, Daphna Shohamy, Neil
1454 Burgess, and Nathaniel D. Daw. 2019. "Hippocampal Contributions to Model-Based Planning and Spatial
1455 Memory." *Neuron* 102 (3): 683-693.e4.
- 1456 Villoutreix, Romain, Diego Ayala, Mathieu Joron, Zachariah Gompert, Jeffrey L. Feder, and Patrik Nosil. 2021.
1457 "Inversion Breakpoints and the Evolution of Supergenes." *Molecular Ecology* 30 (12): 2738–55.
- 1458 Walton, Clare, Eben Pariser, and Fernando Nottebohm. 2012. "The Zebra Finch Paradox: Song Is Little
1459 Changed, but Number of Neurons Doubles." *The Journal of Neuroscience: The Official Journal of the Society
1460 for Neuroscience* 32 (3): 761–74.
- 1461 Wilson, Daniel J. 2019. "The Harmonic Mean P-Value for Combining Dependent Tests." *Proceedings of the
1462 National Academy of Sciences of the United States of America* 116 (4): 1195–1200.
- 1463 Wu, Melody V., Devanand S. Manoli, Eleanor J. Fraser, Jennifer K. Coats, Jessica Tollkuhn, Shin-Ichiro Honda,
1464 Nobuhiro Harada, and Nirao M. Shah. 2009. "Estrogen Masculinizes Neural Pathways and Sex-Specific
1465 Behaviors." *Cell* 139 (1): 61–72.
- 1466 Wu, Ye Emily, Lin Pan, Yanning Zuo, Xinmin Li, and Weizhe Hong. 2017. "Detecting Activated Cell Populations
1467 Using Single-Cell RNA-Seq." *Neuron* 96 (2): 313-329.e6.
- 1468 Xie, Yuanyuan, and Richard I. Dorsky. 2017. "Development of the Hypothalamus: Conservation, Modification
1469 and Innovation." *Development* 144 (9): 1588–99.
- 1470 York, Ryan A., Chinar Patil, Kawther Abdilleh, Zachary V. Johnson, Matthew A. Conte, Martin J. Genner, Patrick
1471 T. McGrath, Hunter B. Fraser, Russell D. Fernald, and J. Todd Strelman. 2018. "Behavior-Dependent Cis
1472 Regulation Reveals Genes and Pathways Associated with Bower Building in Cichlid Fishes." *Proceedings of
1473 the National Academy of Sciences of the United States of America* 115 (47): E11081–90.
- 1474 York, Ryan A., Chinar Patil, C. Darrin Hulsey, J. Todd Strelman, and Russell D. Fernald. 2015. "Evolution of
1475 Bower Building in Lake Malawi Cichlid Fish: Phylogeny, Morphology, and Behavior." *Frontiers in Ecology and
1476 Evolution* 3 (February). <https://doi.org/10.3389/fevo.2015.00018>.
- 1477 Yu, Qingzhao, and Bin Li. 2017. "Mma: An R Package for Mediation Analysis with Multiple Mediators." *Journal
1478 of Open Research Software* 5 (1): 11.
- 1479 Yu, Xinzhu, Anna M. W. Taylor, Jun Nagai, Peyman Golshani, Christopher J. Evans, Giovanni Coppola, and
1480 Baljit S. Khakh. 2018. "Reducing Astrocyte Calcium Signaling in Vivo Alters Striatal Microcircuits and Causes
1481 Repetitive Behavior." *Neuron* 99 (6): 1170-1187.e9.
- 1482 Zhang, Gaoqun, Luisa Lübke, Fushun Chen, Tanja Beil, Masanari Takamiya, Nicolas Diotel, Uwe Strähle, and
1483 Sepand Rastegar. 2021. "Neuron-Radial Glial Cell Communication via BMP/Id1 Signaling Is Key to Long-Term
1484 Maintenance of the Regenerative Capacity of the Adult Zebrafish Telencephalon." *Cells (Basel, Switzerland)*
1485 10 (10): 2794.
- 1486 Zhang, Meng, Stephen W. Eichhorn, Brian Zingg, Zizhen Yao, Kaelan Cotter, Hongkui Zeng, Hongwei Dong,
1487 and Xiaowei Zhuang. 2021. "Spatially Resolved Cell Atlas of the Mouse Primary Motor Cortex by MERFISH."
1488 *Nature* 598 (7879): 137–43.

- 1489 Zhao, Wei-Jiang, San-Jun Yi, Guan-Yong Ou, and Xin-Yu Qiao. 2021. "Neuregulin 2 (NRG2) Is Expressed in
1490 Gliomas and Promotes Migration of Human Glioma Cells." *Folia Neuropathologica* 59 (2): 189–97.
- 1491 Zhao, Y., H. Z. Sheng, R. Amini, A. Grinberg, E. Lee, S. Huang, M. Taira, and H. Westphal. 1999. "Control of
1492 Hippocampal Morphogenesis and Neuronal Differentiation by the LIM Homeobox Gene Lhx5." *Science (New
1493 York, N.Y.)* 284 (5417): 1155–58.